Mafic replenishment of multiple felsic reservoirs at the Mono domes and Mono Lake islands, California

Brandon Bray[1], John Stix[1], and Brian Cousens[2]

1. Department of Earth & Planetary Sciences, McGill University, 3450 University Street, Montreal, Quebec H3A 0E8, Canada

2. Ottawa-Carleton Geoscience Centre, Department of Earth Sciences, Carleton University, 1125 Colonel By Drive, Ottawa, Ontario K1S 5B6, Canada

Abstract

The Mono Basin has been the site of frequent volcanic activity over the past 60,000 years, including the emplacement of the Mono domes and Mono Lake islands. The Mono Basin lavas are the youngest and most poorly understood products of the Long Valley Volcanic Field. We have undertaken a study of Mono Basin volcanism encompassing whole-rock major and trace element, Sr, Nd, Pb, and O isotopic, and electron microprobe glass, plagioclase, and amphibole analyses. Variations in major and trace elements suggest that fractional crystallization of feldspar (Sr, K_2O), apatite (P_2O_5), titanomagnetite (V), zircon (Zr), and allanite (La, Ce) has influenced the evolution of the Mono Basin lavas. Field observations, petrography, and chemistry together demonstrate that injection of more mafic magma is a common process throughout the Mono Basin. Mafic enclaves of the Mono domes are stretched and rounded, with chilled margins between enclave and host rhyolite. Thin sections reveal millimeter-scale inclusions of rhyolite in the enclaves and vice versa along the host-enclave border. Paoha Island dacite has glass with 67-72 wt.% SiO_2 and contains microscopic clots of more mafic glasses, with SiO_2 contents as low as 64 wt.%. Isotopically, the June Lake and Black Point basalts and the Mono dome enclaves represent the least evolved material in the Long Valley Volcanic Field, with $^{87}Sr/^{86}Sr_i$ <0.7056 and $^{143}Nd/^{144}Nd$ >0.5126. The silicic Mono Lake lavas and Mono dome rhyolites display a significant crustal component, with $^{87}Sr/^{86}Sr_i$ >0.7058 and $^{143}Nd/^{144}Nd$ <0.5127. Oxygen and Pb isotopes throughout the sample suite also have crustal signatures, with $^{206}Pb/^{204}Pb$ >19 and $\delta^{18}O$ >+6.5‰. The Mono Lake lavas generally are younger and less evolved than the Mono domes, with enrichment in trace elements including Ba and Sr accompanied by lower $^{143}Nd/^{144}Nd$ and higher $^{206}Pb/^{204}Pb$. This implies that the Mono domes and the Mono Lake lavas are derived from different magma batches, if not from separate magma chambers. There is no systematic relationship between the degree of chemical evolution and the lava ages, indicating that several magma batches have been involved in the development of the Mono domes complex. Pronounced differences in trace element composition (Nb, Y) and isotopic values between the Negit Island and Paoha Island lavas indicate that they, too, are produced by the evolution of at least two different batches of intermediate-composition magma.

Keywords: Mono Lake; Mono domes; mafic enclaves; isotope geochemistry; mafic recharge; rhyolite magmas

1. Introduction

Concern over the possibility of renewed volcanic activity in the Long Valley Volcanic Field began after seismic and magmatic unrest in the region started in 1980 (Hill et al. 1985). The volcanic and tectonic history of the region has since been well established, particularly by Bailey (1989), in order to better assess the potential for future eruptions within and near Long Valley caldera, and the hazards that would be posed by those eruptions. Long Valley caldera was formed during the catastrophic Bishop Tuff eruption of 0.77 Ma (Crowley et al. 2007). Over the past 60,000 years, the focus of magmatic instability has shifted to the north of the caldera into the Mono Basin, where an extensive series of high-silica pyroclastic rocks and lava domes and several basalt flows have been erupted.

Among the Mono Basin volcanic units are several of abnormal composition and ambiguous origin that have important implications for the origin of the entire system. The oldest of the Mono domes, a porphyritic dacite profuse with basaltic enclaves, predates all other domes by nearly 20,000 years (Wood 1983). Several other, younger domes contain abundant enclaves of basalt and andesite (Kelleher and Cameron 1990). Lavas exposed on islands in Mono Lake are mostly dacitic in composition, representing the only intermediate-composition magma generated in the Long Valley region in the past 60,000 years outside of Mammoth Mountain (Hildreth et al. 2014). The Mono Lake lavas are the youngest in the region.

Despite the enigmatic compositions and youth of many of the Mono Basin rhyolites and dacites, their petrogenesis and their relationship to neighboring igneous systems remain poorly understood. This study aims to better understand Mono volcanism through the study of mafic enclaves and silicic volcanic rocks from the Mono Lake islands, and to use the whole-rock and isotope chemistry of these rocks to examine the igneous processes currently occurring in the Mono Basin.

2. Magmatism in the Mono Basin

Activity in the Mono Basin has been for the most part bimodal, but is dominated by high-silica rhyolite. Sarna-Wojcicki et al. (1988) presented evidence of Mono Basin tephras aged 50 to 150 ka and Vazquez and Lidzbarski (2012) found zircon cores dated to 90 ka, although Mono Basin magmatism began in earnest some time later. Starting at ~60 ka, a series of high-silica rhyolites, with one dacite, erupted explosively, each eruption culminating with the emplacement of a lava dome (Fig. 1b; Kelleher 1986; Kelleher and Cameron 1990; Bailey 2004; Vazquez and Lidzbarski 2012). Collectively, this suite is referred to as the Mono domes. Mafic rocks at June Lake and Black Point are interspersed chronologically among these domes. The recent work of Peacock et al. (2015) appears to have confirmed the presence of at least two magmatic sources beneath the Mono Basin, as was proposed by Dawson et al. (1990). Achauer et al. (1986) initially suggested that a substantial, partially molten magma chamber exists beneath the Mono Basin and is the likely source of these recent lavas as regional magma production has shifted to the north of Long Valley caldera.

Through field relationships and hydration rind ages of the Mono domes several early studies concluded that, in general, the mineralogy and geochemistry of the Mono domes correspond chronologically with the typical progression that would be expected from a system undergoing fractional crystallization (Wood 1983; Bursik and Sieh 1989;

Kelleher and Cameron 1990). Recent work on the Wilson Creek tephra section has placed the domes into a more precise chronology (Zimmerman et al. 2011; Vazquez and Lidzbarski 2012; Marcaida et al. 2014). This work broadly agrees with the chronology established by Kelleher and Cameron (1990) based on dome petrology.

Using the dome numbering system of Wood (1983) and the petrological classification scheme of Kelleher and Cameron (1990), as will be utilized throughout this study, dome 12 is the oldest dome, estimated to be >60 ka, and is of dacitic composition. Dome 12 is replete with basaltic enclaves. The next eruptions in the region involved biotite-rich, porphyritic rhyolites (domes 11, 19, and 24), established by hydration rind dates to have been emplaced around 13 ka (Wood 1983). Between 13 and 7 ka, a pair of andesitic enclave- and orthopyroxene-bearing, porphyritic rhyolite domes (domes 14 and 18) erupted first, followed by a more extensive series of porphyritic, fayalite-bearing rhyolite domes (domes 6, 15, 17, 20, 25, and 27-30). Single crystal $^{40}Ar/^{39}Ar$ dating of sanidines found in domes 27-30 by Hu et al. (1994) places these domes at ~13 ka, coincident with the older extreme of this timeline. From roughly 7 until 1.2 ka, volcanism in the Mono Basin was dominated by the eruption of sparsely porphyritic, high-silica rhyolite in the form of dome 8 (often referred to as the Northwest Coulée) and domes 10, 16, 21, 23, and 26. South of the Mono domes are North Deadman Creek dome and Wilson Butte, which are enclave-bearing, sparsely porphyritic rhyolites estimated to have been emplaced at 5039-5297 cal BP and 1611-1710 cal BP, respectively (Fig. 1b; Wood 1983; Miller 1985; Bursik and Sieh 2013). Although these two domes are geographically located within the Inyo dome suite, Lajoie (1968) and Bailey (1989) classified both as members of the Mono domes suite. The geochemical data presented in this study support this classification. In the past 1200 years, two voluminous pulses of aphyric, high-silica rhyolite volcanism have occurred. The first pulse was at 1366-1420 cal BP, emplacing dome 22 – the South Coulée – and the second pulse occurred at 600-625 cal BP, emplacing dome 3 – Panum Crater – and domes 4, 5, 7, 9, and 13 – the North Coulée (Bursik and Sieh 2013; Bursik et al. 2014). The latter event is commonly referred to as the North Mono eruption (Sieh and Bursik 1986; Hildreth 2004). Tephra produced during the explosive phases of these eruptions blankets most of the older domes (Vazquez and Lidzbarski 2012).

Coeval with dome emplacement are the June Lake and Black Point basalts. Between 30 and 25 ka, the June Lake basalt flowed from a cinder cone near June Lake, located in the southwestern Mono Basin (Bursik and Gillespie 1993; Bailey 2004). While the biotite-bearing Mono domes were being emplaced, at roughly 16-17 ka, the Black Point basalt was erupted subaqueously into Pleistocene Mono Lake, taking the form of a flat-topped cinder cone (Lajoie 1968; White 2000; Bailey 2004).

Concurrent with the eruption of aphyric rhyolite in the Mono Basin was the commencement of sparsely porphyritic dacitic volcanism in Mono Lake, a 15 km x 21 km lake located north of the Mono domes (Stine 1987; Bailey 2004). The initial locus of Mono Lake volcanism was Negit Island, which is dominated by a dacitic cinder cone and several dacitic lava flows originating therein. Stine (1987) estimated that Negit Island was active from 1.7 to 0.4 ka based on the presence of tephra layers from three of the more recent Mono dome eruptions: two tephras established by Wood (1983) to be ~1.6 and 1.2 ka, and a third tephra dated to 0.6 ka according to Sieh and Bursik (1986). Further outcrops of these dacite flows are seen to the north of Negit Island on a series of small islands referred to here as the Negit islets. Following the last eruption on Negit Island, an intrusion beneath the central part of Mono Lake caused updoming of a significant volume of lake sediment and the eruption of a small volume of dacite, including cinder cones and lava flows, forming present-day Paoha Island (Stine 1987; Kelleher and Cameron 1990). Between 500 and 150 years ago, low-silica rhyolite lava was erupted in the northwestern quadrant of Paoha Island; these appear to be the most recent eruptions in the Long Valley Volcanic Field. Stine (1987) placed these limits on Paoha Island's emplacement based on prehistoric lake levels and the presence of sedimentary features that would have been eroded easily by submergence.

3. Methodology

3.1 Fieldwork

During two field seasons, in October 2011 and July-August 2012, sampling focused on the Mono Lake islands; the Mono domes; the Mono dome enclaves; the June Lake and Black Point basalts; and South Deadman Creek Dome, the southernmost of the Inyo domes (Fig. 1; Table 1).

3.2 Whole-rock major and trace element and isotopic geochemistry

Rock chips from fifty-four samples, covering the Mono Lake islands, the Mono domes, all mafic enclave populations, and local basalts, were analyzed for major and trace elements by X-ray fluorescence (XRF) at the Washington State University GeoAnalytical Lab (techniques of Johnson et al. 1999). For major elements, reported analytical precision is within <1 wt. %; trace element analyses are precise to within 2 parts per million (ppm) (Johnson et al. 1999). Several powders of the UTR-2 standard were included in each batch of XRF samples to further gauge the accuracy and precision of the analyses (Online Resource 1). Since some mafic enclaves show evidence of mingling with felsic magmas along their margins, only material from the cores of the enclaves was crushed for geochemical analysis. As most rocks from Mono Lake were at one point submerged, rock chips from samples collected near the present, historically low lake level during the 2011 field season were cleaned using acetic acid and deionized water. Repeat analyses comparing cleaned samples to uncleaned splits of the same samples show that cleaning had a negligible effect (Online Resource 1). This implies that the waters of Mono Lake have had little, if any, effect on the trace element composition of the Mono Lake lavas, so the samples collected in the 2012 field season were rinsed only with deionized water.

Rock powders of sixteen representative samples were then selected for Sr, Nd, and Pb isotopic analyses at the Carleton University Isotope Geochemistry and Geochronology Research Centre (IGGRC). Samples were chosen to ensure geographic and compositional coverage, with a particular focus on the enclaves and islands. Elemental separation techniques were those of Cousens (1996), and samples were run on a ThermoFinnigan Triton TI thermal ionization mass spectrometer. All Pb mass spectrometer runs are corrected for fractionation using NIST SRM981. The average ratios measured for SRM981 are $^{206}Pb/^{204}Pb = 16.889 + 0.007$, $^{207}Pb/^{204}Pb = 15.426 + 0.009$, and $^{208}Pb/^{204}Pb = 36.494 + 0.031$, based on 35 runs between May 2008 and May 2011. The fractionation correction is +0.13%/amu (based on the values of Todt et al. 1996). Sr isotope ratios are normalized to $^{86}Sr/^{88}Sr = 0.11940$. Two Sr standards were run at Carleton University, NIST SRM987 ($^{87}Sr/^{86}Sr = 0.710239 + 14$, n=20, May 2008-2011) and the Eimer and Amend (E&A) $SrCO_3$ ($^{87}Sr/^{86}Sr$ = 0.708012 + 15, n=10, Sept. 2007-May 2011). Nd isotope ratios were normalized to $^{146}Nd/^{144}Nd$ = 0.72190. Analyses of the USGS standard BCR-1 yield $^{143}Nd/^{144}Nd$ = 0.512668 + 20 (n=4). A total of 30 runs of an internal Nd metal standard average $^{143}Nd/^{144}Nd$ = 0.511823 + 12, corresponding to a La Jolla value of 0.511852 based on comparative runs (May 2008-2011). All quoted uncertainties are 2-sigma standard deviations of the mean.

This same subset of whole-rock powders, in addition to the June Lake and Black Point basalts, was analyzed for $^{18}O/^{16}O$ stable oxygen isotopes at the Queen's University Facility for Isotope Research (QFIR) on a Finnigan MAT 252 Isotope Ratio Mass Spectrometer (IRMS). Gas for $^{18}O/^{16}O$ analysis was extracted from 5 mg samples of rock powder using the BrF_5 reaction method of Clayton and Mayeda (1963) on the QFIR silicate extraction line. Reproducibility of $\delta^{18}O$ values is ±0.3 ‰.

3.3 Electron microprobe analysis

Electron microprobe analyses of amphibole, plagioclase, and volcanic glass in polished thin sections were conducted at McGill University using a JEOL 8900 electron microprobe. Glass analyses were conducted using a 15 kV accelerating voltage, an 8 mA beam current, and a 20 μm beam diameter, to prevent Na_2O loss. Glass standards BMAK and KE-12 were used to calibrate Mg, Fe, Ca, and Ti; and Na, Al, Si, and K, respectively. Manganese and phosphorous were calibrated using synthetic standards. The PCD and M3N standards were analyzed after each sample to gauge instrumental accuracy (Online Resource 1). Since PCD has very low H_2O and M3N has relatively high H_2O, these two standards were used to accurately assess variations in the H_2O content of different glasses.

Amphibole analyses used an accelerating voltage of 15 kV, a beam current of 20 mA, and a 10 μm beam diameter. All elements were standardized to a mixture of synthetic standards; results were compared to the HBLD standard to gauge instrumental precision and accuracy.

4. Results

4.1 Field observations, petrology, and mineral chemistry

4.1.1 Mono dome enclaves

The most salient observations from field relationships are those for the centimeter-scale mafic enclaves hosted within Mono domes 12, 14, and 18. The enclaves in domes 14 and 18 vary from black to red in color. Populations of each hue are present in each dome. They are finely vesicular, stretched, and rounded, and commonly have glassy, chilled margins coupled with melting rims in their felsic hosts (Fig. 2). Kelleher and Cameron (1990) noted similar enclave textures. The uniformly red enclaves of dome 12 are generally much smaller, never exceeding five centimeters. Rare andesitic enclaves are also present in Wilson Butte and North Deadman Creek dome.

The dome 12 dacite contains abundant centimeter-scale plagioclase and millimeter-scale hornblende and clinopyroxene crystals. Enclaves of basalt and basaltic andesite within the dacite are vesicular, contain plagioclase, olivine, and clinopyroxene phenocrysts, and range from microscopic to upwards of five centimeters in scale. Owing to the intimate commingling of the enclaves and the host dacite in the samples collected, this study uses the whole-rock analysis of Kelleher and Cameron (1990) for dome 12.

The mafic and intermediate enclaves of domes 14 and 18 are petrographically similar. Millimeter-scale olivine, plagioclase, and orthopyroxene phenocrysts are present in all enclaves. It is common to see microscopic inclusions of solidified rhyolitic magma within the enclaves, and vice versa, along the host-enclave margin (Fig. 6).

4.1.1 Mono Lake lavas

Unique to the Paoha Island lavas are microscopic clots of foreign, possibly more mafic material, in the form of round pockets of glass, plagioclase, and biotite that stand out from the groundmass of the lava (Fig. 4). Amphiboles found in the Mono Lake lavas are fairly uniform in composition, with SiO_2 varying from 41.2 to 42.5 wt.%, FeO_T from 12.6 to 17.4 wt.%, and MgO from 10.8 to 13.9 wt.% (Fig. 13a; Table 4b). All Mono Lake amphiboles plot as tschermakite, reflecting their relatively low Fe contents (Fig. 13a). In comparison, amphiboles from the Inyo domes plot as magnesio-hornblende and are more enriched in Fe. No systematic variation is apparent between rims and cores of hornblende crystals. Thermobarometric calculations using the formulae of Ridolfi et al. (2009) indicate that the Mono Lake amphiboles were formed at temperatures of ~915-1000°C and pressures of 245-325 MPa (Fig. 13b). The Inyo dome amphiboles, including amphiboles in the Inyo dome enclaves, were formed at temperatures of ~780-915°C and pressures of 75-260 MPa.

Regardless of the location, whether a sample is from the Mono domes, Mono Lake, or a mafic enclave, most plagioclase phenocrysts exhibit pronounced dissolution textures (Fig. 5). For example, otherwise euhedral plagioclase crystals appear to be dissolving into the host rhyolite along their rims. Phenocrysts commonly have spectacular sieve textures, with almost the entire crystal pockmarked (Fig. 5a-b). Many of the voids have been filled subsequently with glass and microlites, although most remain vacant. The sieve texture is commonly coupled with distinct overgrowth rims, suggesting that renewed crystallization of feldspar from the felsic magmas occurred as they cooled. These textures imply that reheating of the felsic magma occurred, and that this is a common petrogenetic process occurring at depth throughout the Mono Basin.

4.2 Whole-rock major and trace element and glass geochemistry

Silica shows strong positive correlations with K_2O and Rb (Fig. 7; Table 2). As it is the most incompatible element analyzed, Rb is used as an index of differentiation in all other geochemical plots (Figs. 8-10). Throughout the sample suite, pronounced fractionation trends are present in elements such as P, K, Sr, V, and Zr (Fig. 8). These trends underpin the important role played by the crystallization of plagioclase, as well as accessory mineral phases such as zircon, apatite, titanomagnetite, and allanite (Kelleher and Cameron 1990, Vazquez and Lidzbarski 2012).

In major element space, the Mono domes lie within a very narrow compositional range. The variation in SiO_2 concentration is between 75 and 77 wt.% on an anhydrous basis; all other major elements are similarly uniform (Table 2). The minor increase in SiO_2 content in the Mono domes corresponds to the temporal evolution from biotite-bearing lavas to orthopyroxene-bearing lavas, fayalite-bearing lavas, porphyritic lavas lacking any unique ferromagnesian mineral phases, and, finally, aphyric lavas.

The Mono Lake islands, on the other hand, are quite varied in major element composition and are less evolved than the Mono domes, in spite of their comparative youth. On Paoha Island, SiO_2 varies from 63 to 72 wt.%, while Negit Island and the Negit islets display a range from 64 to 70 wt.% SiO_2. In general, K_2O increases with SiO_2, except in the Mono domes, which are depleted in K_2O relative to the most evolved Paoha Island rhyolites (Fig. 7a). All other major element concentrations decrease with increasing SiO_2.

Trace elements are more useful in differentiating among the different mineralogical types of Mono domes, as established by Kelleher and Cameron (1990). Domes 14 and 18, the orthopyroxene- and enclave-bearing porphyritic rhyolites, are the most depleted in Rb, with 156 and 164 ppm, respectively. They are also depleted in Nb and Y compared to the rest of the Mono domes (Fig. 9) and enriched in Zr, La, and Ce (Figs. 8d, 9c-d). At first glance, the considerable range in La (18 to 38 ppm) and Ce (42 to 69 ppm) concentrations within the remaining domes would appear to further distinguish them; careful examination, however, reveals that the variations in La and Ce do not correspond to geography, mineralogy, or major element composition.

The Mono Lake lavas display significant trace element variations and are overall less evolved than the Mono domes. The lavas of Mono Lake have higher, more variable Ba concentrations when compared to all other Mono Basin lavas, ranging from 1000 to 1600 ppm, and Sr concentrations from 95 to 530 ppm (Fig. 10; Table 2). Similarly, they are conspicuously depleted in Rb relative to the Mono domes, with concentrations ranging from 100 to 130 ppm. For comparison, within the Mono domes, Sr ranges from 1 to 25 ppm, Ba from 10 to 40 ppm, and Rb from 130 to 180 ppm (Fig. 10).

The Negit and Paoha lavas exhibit marked differences from one another. Among the high field strength elements, particularly Y and Nb, Negit and Paoha lavas define discrete fields with no overlap, suggesting that the islands are chemically distinct (Fig. 9). The older Negit lavas have Y and Nb concentrations reflective of a less evolved magma

(18 to 20 ppm and 12 to 14 ppm, respectively), while the more youthful Paoha lavas are comparatively enriched in Y and Nb (19 to 27 ppm and 15 to 19 ppm, respectively).

Examining the new geochemical data presented here combined with those of Kelleher and Cameron (1990) shows that the basaltic enclaves from dome 12 vary little from one another: SiO_2 ranges from 50 to 54 wt.%, notably lower than the enclaves from domes 14 and 18, and the other elements analyzed exhibited no systematic variation (Table 2). The dome 14 and 18 enclaves define two distinct populations chemically and petrologically (Figs. 7-10). In each dome, one set of enclaves has 55 to 56 wt.% SiO_2, while another set has 59 to 61 wt.% SiO_2, with correlative variations in the other major and trace elements. The two enclave populations form distinct clusters in most major and trace element diagrams. A fractionation trend between the two populations is often apparent, particularly in trace elements such as Rb and Sr (Fig. 10a). The Inyo and North Deadman Creek dome enclaves analyzed in this study and by Varga et al. (1990) had compositions more similar to the Mono Lake dacites than to the other Mono enclaves, with SiO_2 of 60 to 62 wt.% and enriched Rb and Ba concentrations compared to the enclaves of domes 12, 14, and 18 (Figs. 8-10; Table 2).

The enclave-bearing Mono dome lavas also have millimeter-scale inclusions of glass that are more mafic than the host rhyolite, with SiO_2 contents of 49 to 55 wt.%, CaO contents in excess of 8 wt.%, and K_2O contents less than 2 wt.% (Fig. 12c-d; Table 4a). On Paoha Island, where the host glass compositions are dominantly felsic, with SiO_2 of 67 to 72 wt.%, CaO less than 2 wt.%, and K_2O greater than 4 wt.%, microscopic clots of more mafic glass have SiO_2 concentrations as low as 64 wt.%, CaO up to 3.3 wt.%, and K_2O as low as 3.5 wt.% (Figs. 4, 12a-b; Table 4a). These clots contain glass, plagioclase, and biotite, and appear to be unique to Paoha Island (Fig. 4).

4.3 Radiogenic isotopes

Within the Mono domes, $^{87}Sr/^{86}Sr_i$ presents a range from 0.70596-0.70690, and $^{143}Nd/^{144}Nd$ from 0.51260 to 0.51262 (Fig. 11). The Mono Lake lavas are similar, with $^{87}Sr/^{86}Sr_i$ from 0.70587-0.70642, and $^{143}Nd/^{144}Nd$ from 0.51252 to 0.51259. The mafic enclaves present within the Mono domes display a range of $^{87}Sr/^{86}Sr_i$ from 0.70442 to 0.70486, significantly lower than the silicic Mono lavas, and $^{143}Nd/^{144}Nd$ from 0.51274 to 0.51278, well above other values for silicic rocks in the Mono Basin. The exceptions are the enclaves of the Inyo domes analyzed here and by Varga et al. (1990), which have radiogenic isotopic ratios resembling the Negit Island dacites ($^{87}Sr/^{86}Sr_i$ 0.70622, $^{143}Nd/^{144}Nd$ 0.51252), and the enclaves of North Deadman Creek dome ($^{87}Sr/^{86}Sr_i$ 0.70564, $^{143}Nd/^{144}Nd$ 0.51264). The entire sample suite has a very tight range of Pb isotopic values, all reflecting a crustal or sedimentary signature; $^{208}Pb/^{204}Pb$ ranges from 38.86 to 39.04, $^{207}Pb/^{204}Pb$ from 15.66 to 15.71, and $^{206}Pb/^{204}Pb$ from 19.09 to 19.24 (Fig. 11; Table 3).

4.4 Oxygen isotopes

The range in our $\delta^{18}O$ values is +6.5 to +9.5‰, with two exceptions: a peperite sample from Paoha Island with $\delta^{18}O$ of +11.6‰, likely due to integration of sediment into the dacites in the locality at which this sample was taken; and a dome 18 enclave with $\delta^{18}O$ of +12.7‰ (Table 3). There is no correlation between loss on ignition from the XRF analyses and $\delta^{18}O$. The overall $\delta^{18}O$ range is characteristic of crustal compositions in general, as reported by Bindeman (2008) as +5 to +18‰, and furthermore coincides with the range of Eastern Sierra Nevada basement whole-rock oxygen isotope values presented by Lackey et al. (2008) of +7.0 to +9.5‰. That said, there are notable variations within the new oxygen isotope data presented here. The Mono domes, rather than defining a tight cluster as they do for other chemical components, range from +6.9 to +9.0‰; similarly, the Paoha Island lavas vary from +7.6 to +9.4‰, ignoring the abnormally elevated sample from the Paoha peperite.

5. Discussion

The data presented above offer several implications regarding the petrogenetic processes involved in the generation of the Mono Basin lavas, as well as their context within the Long Valley Volcanic Field as a whole. In addition to fractional crystallization, as detailed above, these processes include interaction with both mafic intrusions and the felsic Sierra Nevada crust. We now discuss these aspects in detail.

5.1 Basalt-rhyolite and magma-crust interactions in the Mono Basin

The Mono dome enclaves display clear evidence of having been at least partially molten upon incorporation into the Mono domes rhyolite. They are vesicular, rounded, and have chilled margins (Fig. 2). Field and petrographic observations of the Mono domes suggest that mingling between the mafic enclaves and their felsic hosts has occurred. Examination of inclusions along the enclave-host margin reveals microscopic clots of each magma type contained within the other (Fig. 6). For example, while the groundmass glass of the dome 14 andesitic enclaves has 60 wt.% SiO_2, 6 wt.% CaO, and less than 2 wt.% K_2O, millimeter-scale globules of rhyolite found within the enclaves have nearly 77 wt.% SiO_2, less than 1 wt.% CaO, and nearly 6 wt.% K_2O (Fig. 12c-d;

Table 4a). For this reason, the rock chips used for whole-rock major and trace element and isotope geochemistry of the enclaves were taken from their cores.

The presence of mafic enclaves in the Mono dome rhyolites is a direct line of evidence revealing that mafic magmas have co-existed and interacted with the silicic magma. The enclaves are intermediate in composition between the host rhyolites and regional mafic material; hence this material likely represents fractional crystallization of basalt that intruded into the felsic magma, at which point some mixing between the Mono dome rhyolites and intruding magma may have occurred, in addition to the magma mingling described above (Fig. 12c-d). Lever rule calculations using the June Lake basalt as a mafic end member, domes 14 and 18 as felsic end members, and each dome's enclaves as intermediate compositions show the enclaves to represent a mixture of 75-80% mafic material and 20-25% felsic material, however the textural evidence does not support magma mixing to this extent. The relationship between regional basalts, enclaves, and the Mono dome lavas is far from linear, an observation that is reflective of crystallization of both the mafic and felsic magmas over thousands of years as well as the existence of multiple magma sources beneath the Mono Basin. This latter conclusion is consistent with the conclusions of Dawson et al. (1990) and Peacock et al. (2015), who propose that multiple magma sources exist beneath the Mono Basin, as will be discussed further below.

In contrast to the Mono domes, there is little direct petrological evidence of basaltic magma input into the Mono Lake magmas, yet the clots in the Paoha Island lavas are significant. The clots are only slightly less silicic than their host lavas, compared to the Mono dome enclaves (Fig. 12a-b). Mono Lake magmas may be replenished by intermediate magma, or, alternatively, small volumes of intruding basalt may be mixed efficiently with larger volumes of Mono Lake dacite. The latter hypothesis seems the most likely case, as the Black Point basalt is not only adjacent to Mono Lake, but also provides a fitting parental end member for the Mono Lake lavas (Figs. 7-10).

The pervasive disequilibrium textures visible in plagioclase phenocrysts further demonstrate that mafic rejuvenation is a common process beneath the Mono Basin. Even in lavas with no other physical evidence of basaltic recharge, plagioclase phenocrysts have sieve textures and overgrowth rims (Fig. 5). Although the formation of sieve textures and overgrowth rims in feldspars during decompression and subsequent crystallization is a well-established phenomenon, the sieve textures which we observe coincide with other observational evidence of magma mixing in the Mono Basin lavas, as discussed above (Nelson and Montana 1992, Blundy et al. 2006). The partial dissolution of crystals, and their subsequent overgrowth rims, indicates the reheating of the felsic host rock, which in turn implies intrusion of a hotter, mafic magma.

Isotopic data indicate that magma-crust interaction is also an important process in the evolution of the Mono Basin magmas. While $^{87}Sr/^{86}Sr$ and $^{143}Nd/^{144}Nd$ ratios preserve mantle signatures in the basalts and mafic enclaves, the silicic rocks of the Mono domes and Mono Lake have significantly more crustal signatures, with $^{87}Sr/^{86}Sr_i$ straddling the 0.706 line that appears to separate the Mono Basin basalts and enclaves from all other regional lavas (Fig. 11a; Table 3). The mantle signatures of the mafic enclaves suggest that limited chemical exchange occurred between mafic magmas and host rocks, while the lithospheric signatures of the silicic rocks suggest that substantial crustal input has occurred throughout the system. This is reinforced by our Pb and O isotopic data, which convey strong crustal signatures throughout the sample suite (Fig. 11; Lackey et al. 2008). Notably, Pb and O isotopic values do not correlate with volatile content, indicating that they are truly reflective of crustal contamination. This is true even among the Mono Lake lavas, which have had prolonged, intimate contact with the lake's water that could have affected Pb and O isotope values.

Mafic recharge is the most likely explanation for the presence of the mafic enclaves, their textures and mineral chemistries, and the mantle-crustal mixing isotopic signatures observed throughout the Mono domes and Mono Lake island lavas. Mafic parental magmas partially melt Sierra Nevada basement rocks, which then lie dormant in shallow reservoirs, evolving until intruded by hot mafic magma. This intrusive magma mixes and mingles with the preexisting, crustal felsic magma and facilitates its eruption, a process that has been well established in large, silicic igneous systems (e.g., Sparks et al. 1977; Bailey 2004). The influx of hot magma into the crust encourages further partial melting of basement rock, promoting the evolution of silicic magmas with crustal isotopic signatures. The remaining magmas continue crystallizing and interacting until the next intrusion of basalt, when the process repeats.

5.2 Separate sources of the Mono domes and Mono Lake magmas

While the Mono Lake lavas are generally younger than the Mono domes, they are also significantly less evolved. In addition to the obvious differences in SiO_2 content and other major elements, the lavas of Paoha and Negit are markedly enriched in trace elements such as Ba and Sr compared to the Mono domes (Figs. 9-10). With the exception of one sample from Paoha Island, Mono Lake lavas have lower $^{143}Nd/^{144}Nd$ and slightly higher $^{206}Pb/^{204}Pb$ than the Mono dome rhyolites (Fig. 11; Table 3).

The eruption of dacites and low-silica rhyolites in Mono Lake is a reversal of the chemical trend that dominated the Mono Basin for the preceding 60,000 years, in which successive eruptions were generally more silicic and more evolved than preceding eruptions. The implication is that even if the mantle source of the Mono dome and Mono Lake magmas is the same, each suite represents a different batch of magma that has been variably affected by basaltic rejuvenation, fractional crystallization, and crustal contamination, and possibly storage in entirely separate magma chambers. Notably, the Mono Lake magmas appear to be derived from a hot (915-1000°C) and deep (245-325 MPa) reservoir, based on our amphibole thermobarometric data (Fig. 13b; Ridolfi et al. 2009).

Bailey (2004) theorized that the postcaldera dacites erupted within and proximal to Long Valley caldera, including the Mammoth Mountain dacite and the Mono dacites, have likely formed from a number of discrete magma batches in separate subsurface chambers. This is consistent with the chemical and physical diversity noted here between the Mono dome dacite (dome 12) and the Mono Lake dacites, as well as the theorized presence of a magma chamber beneath the Mono Basin that is separate from the Long Valley caldera chamber and fuels several shallow magma reservoirs (Achauer et al. 1986; Dawson et al. 1990; Peacock et al. 2015). The older lavas of each suite (dome 12 and Negit Island) thus may reflect two separate batches of dacitic magma, likely formed by fractional crystallization of mantle-sourced basalt and partial melting of the Sierra Nevada basement (Kelleher and Cameron 1990; Hildreth 2004).

Furthermore, Negit Island and Paoha Island are themselves potentially the products of discrete magma batches (Kelleher and Cameron 1990). All of the Negit lavas have slightly higher $^{87}Sr/^{86}Sr_i$ and $^{206}Pb/^{204}Pb$ ratios than the Paoha lavas (Fig. 11b; Table 3). Negit Island also has pronouncedly lower Nb and Y concentrations (Fig. 9a-b; Table 2). The trace element and radiogenic isotope signatures together indicate that the Negit flows, arguably the older of the lavas, were produced from a different felsic magma than the Paoha flows.

The idea that several distinct magma batches were produced and erupted is not unique to Mono Lake. Indeed, it appears likely to have occurred in the Mono domes as well, as is supported by chemical evidence. For almost all elements, three individual clusters of rhyolitic domes can be seen, with notable compositional gaps between each cluster (Figs. 7-10). These dome clusters do not correspond temporally, meaning that they cannot reflect the evolution of a single batch of magma. There is no systematic relationship between the age of a dome cluster and its degree of chemical evolution. The majority of Mono dome lavas, including the biotite- and fayalite-bearing, sparsely porphyritic, and aphyric domes, define a continuous array that does not suggest temporal or spatial patterns. The orthopyroxene- and enclave- bearing domes 14 and 18 are consistently less evolved than this large array, but are intermediate in age between the biotite-bearing domes and the other high-silica rhyolites. The least evolved rhyolitic Mono dome is North Deadman Creek dome, notably the southernmost dome of the chain. Bursik and Sieh (2013) calculated the age of North Deadman Creek dome to be between 5039 and 5297 cal BP, chronologically between the two clusters of more evolved domes. Given the lack of chronological correlation present among the three Mono dome clusters, they were likely produced by several magma batches undergoing similar petrogenetic processes.

5.3 Regional context

Wark et al. (2007) provide compelling evidence from quartz cathodoluminescence and thermometry that the Bishop Tuff eruption was stimulated by mafic recharge of the Long Valley magma chamber. Early postcaldera silicic lavas, erupted on the floor of Long Valley caldera from ~0.7 to 0.5 Ma, contain vesicular, rounded mafic magmatic enclaves with chilled margins, similar to those present in the Mono domes (Bailey 2004). These common textures, along with the eruption of post-Bishop Tuff mafic to intermediate lava flows along the caldera margin, indicate that mafic rejuvenation of the Long Valley magma system has been an important process since caldera formation. Seismic activity beneath Long Valley caldera starting in 1980 has been interpreted as basaltic recharge around the Long Valley magma chamber (Hill et al. 1985; Battaglia et al. 1999; Bailey 2004; Hill and Prejean 2005). The present study indicates that the same process occurs beneath the Mono Basin.

The mafic lavas of the Mono Basin, including the Mono dome enclaves and the June Lake and Black Point basalts, exhibit the least radiogenic $^{87}Sr/^{86}Sr_i$ and most radiogenic $^{143}Nd/^{144}Nd$ values of the entire Long Valley Volcanic Field (Fig. 11a). Since any interaction with the felsic host magma could only have elevated $^{87}Sr/^{86}Sr_i$ in the mafic component, the anomalously low $^{87}Sr/^{86}Sr_i$ values in the Mono dome enclaves likely reflect the maximum possible $^{87}Sr/^{86}Sr_i$ of the mafic magma source (Fig. 11a-b). Cousens (1996) suggested that low $^{87}Sr/^{86}Sr_i$ in the Black Point and Red Cones basalts reflects the initiation of asthenospheric melting beneath the Long Valley region; $^{87}Sr/^{86}Sr_i$ in the Mono dome enclaves supports this conclusion.

The enclaves from domes 12, 14, and 18 also show slightly lower $^{206}Pb/^{204}Pb$ compared to the field as a whole (Fig. 11b). By contrast, Sr and Nd isotopic signatures in both precaldera and postcaldera mafic lavas associated with the caldera resemble the Sierra Nevada crust and lithospheric mantle, with the exception of the Black Point and Red Cones lavas (Fig. 11; Online Resource 1; Van Kooten 1981; Cousens 1996). There is a striking difference in $^{206}Pb/^{204}Pb$ between precaldera and postcaldera mafic lavas, with postcaldera basalts and andesites tending towards higher values, hence more pronounced levels of crustal contamination (Fig. 11b). The marked difference between mafic material erupted in and around Long Valley and mafic material in the Mono Basin may indicate that mantle melts are being brought to the surface more efficiently in the Mono Basin than in Long Valley, and that their crustal residence time is shorter. In comparison, the silicic Mono Basin lavas exhibit $^{87}Sr/^{86}Sr_i$ and $^{143}Nd/^{144}Nd$ values comparable to Glass Mountain and the Bishop Tuff (Fig. 11a; Table 3; Online Resource 1; Halliday et al. 1984; Heumann and Davies 1997; Davies and Halliday 1998). This similarity suggests that the processes responsible for the Mono Basin dacites and rhyolites are similar to those that generated the high-silica precaldera and caldera-forming magmas.

While it remains uncertain whether a distinct magma chamber underlies Mono Lake, as was suggested by Pakiser (1960), Achauer et al. (1986), Peacock et al. (2015) provide convincing magnetotelluric evidence that not only does this chamber exist, but it has produced multiple shallow reservoirs beneath the Mono Basin. The propagation of magma reservoirs beneath the Mono Basin and throughout the Long Valley region in general is promoted by the complex regional tectonic regime; the intersection of the Sierra Nevada batholith and Basin and Range extension has provided an ideal environment both for mafic magma intrusion and production of silicic magmas (Bursik et al. 2003; Riley et al. 2012). It is likely, based on our data and that of others, that the Mono domes and Mono Lake lavas are derived from disparate and discrete magma batches, as proposed by Kelleher and Cameron (1990) and Hildreth (2004). Our amphibole thermobarometry results indicate that the Mono Lake dacites and rhyolites are derived from a magma reservoir (or reservoirs) that is fairly deep, i.e., 9-12 km (Fig. 13b; Ridolfi et al. 2009). There is little evidence of Long Valley magma having migrated north to beneath the Mono Basin. The occurrence of Mono domes as far south as Wilson Butte and North Deadman Creek dome, however, supports the theory of Sieh and Bursik (1986) and Varga et al. (1990) that Mono-type magma is one component of the most recent Inyo eruptions.

6. Concluding remarks

Mafic recharge is a well-established mechanism by which volcanic activity in voluminous silicic systems is initiated. More specifically, there is a well-documented body of work indicating that mafic recharge has been an important process in the petrogenesis of lavas throughout the Long Valley Volcanic Field and elsewhere in the northern Sierra Nevada. Our geochemical data indicate that variable amounts of partial melting of the Sierra Nevada crust, fractional crystallization, and magma mixing and mingling have generated the chemical variations observed for the silicic rocks of the Mono Basin. Our field and petrographic observations throughout the study area are consistent with mafic recharge playing a significant and perhaps dominant role in the genesis and evolution of silicic magmas in the Mono Basin. In the case of the Mono domes, the felsic reservoir may be the Mono Basin magma chamber proposed by Pakiser (1960) and Achauer et al. (1986) and supported by Peacock et al. (2015), or a series of distinct reservoirs based on the three groups of Mono dome lavas. In the case of the Mono Lake lavas, the felsic reservoir must have contained either a separate batch of less evolved magma within the Mono Basin chamber or, more likely, dacite stored at mid-crustal levels in a chamber (or chambers) beneath Mono Lake.

Acknowledgements

Dave Marquart of the Mono Lake Tufa State Natural Reserve and Tamara Sasaki of California State Parks were instrumental in ensuring that we received the proper permits needed to explore Negit and Paoha. Dan Dawson, Kim Rose, and the rest of the staff of the Sierra Nevada Aquatic Research Lab provided us with housing and lab space during the 2012 field season. Bartshe Miller and the volunteers of the Mono Lake Committee let us rent their boat on several occasions. Kristie Nelson was a keen observer and faithful companion in the field. Patrick Beaudry and Gregor Lucic were able field assistants in the summer of 2012.

Paul Alexandre, Kristen Feige, and the rest of the Queen’s Facility for Isotope Research staff assisted with oxygen isotope determinations, and Rhea Mitchell at the Carleton Isotope Geochemistry and Geochronology Research Centre was unflagging in her efforts to make sure that we obtained the best radiogenic isotope data possible. Dr. Wes Hildreth of the U.S. Geological Survey read an early draft of this manuscript. We are grateful to him for his comments and suggestions. This research was supported by Discovery and Accelerator grants to J. Stix from the Natural Sciences and Engineering

Research Council of Canada, as well as a grant to B. Bray from the University of California Valentine Eastern Sierra Reserve.

References

Achauer U, Greene L, Evans JR, Iyer HM (1986) Nature of the magma chamber underlying the Mono Craters area, eastern California, as determined from teleseismic travel time residuals. J Geophys Res 91: 13873-13891

Bailey RA (1989) Geologic map of Long Valley caldera, Mono-Inyo Craters volcanic chain, and vicinity, eastern California. US Geol Surv Misc Investig Ser Map I-1933, 11 pp, scale 1:62,500, 2 sheets

Bailey RA (2004) Eruptive history and chemical evolution of the precaldera and postcaldera basalt-dacite sequences, Long Valley, California: implications for magma sources, current seismic unrest, and future volcanism. US Geol Surv Prof Pap 1692, 76 pp

Battaglia M, Roberts C, Segall P (1999) Magma intrusion beneath Long Valley caldera confirmed by temporal changes in gravity. Science 285: 2119-2122

Bindeman I (2008) Oxygen isotopes in mantle and crustal magmas as revealed by single crystal analysis. Rev Mineral Geochem 69: 445-478

Blundy J, Cashman K, Humphreys M (2006) Magma heating by decompression-driven crystallization beneath andesite volcanoes. Nature 443: 76-80

Bursik M, Sieh KE (1989) Range front faulting and volcanism in the Mono Basin, eastern California. J Geophys Res 94: 15587-15609

Bursik MI, Gillespie AR (1993) Late Pleistocene glaciation of Mono Basin, California. Quat Res 39: 24-35

Bursik M, Renshaw C, McCalpin J, Berry M (2003) A volcanotectonic cascade: Activation of range front faulting and eruptions by dike intrusion, Mono Basin ‐ Long Valley Caldera, California. J Geophys Res: Solid Earth 108: B8

Bursik M, Sieh K (2013) Digital database of the Holocene tephras of the Mono-Inyo Craters, California. US Geol Surv Data Ser 758

Bursik M, Sieh K, Meltzner A (2014) Deposits of the most recent eruption in the Southern Mono Craters, California: description, interpretation and implications for regional marker tephras. J Volcanol Geotherm Res 275: 114-131

Chaudet RE (1986) The petrology and geochemistry of precaldera magmas, Long Valley caldera, eastern California. MSc thesis, Virginia Polytechnic Institute

Christensen JN, DePaolo DJ (1993) Time scales of large volume silicic magma systems: Sr isotopic systematics of phenocrysts and glass from the Bishop Tuff, Long Valley, California. Contrib Mineral Petr 113: 100-114

Clayton RN, Mayeda TK (1963) The use of bromine pentafluoride in the extraction of oxygen from oxides and silicates for isotopic analysis. Geochim Cosmochim Acta 27: 43-52

Cousens BL (1996) Magmatic evolution of Quaternary mafic magmas at Long Valley caldera and the Devils Postpile, California: effects of crustal contamination on the lithospheric mantle-derived magmas. J Geophys Res 101: 27673-27689

Crowley JL, Schoene B, Bowring, SA (2007) U-Pb dating of zircon in the Bishop Tuff at the millennial scale. Geology 35: 1123-1126

Davies GR, Halliday AN (1998) Development of the Long Valley rhyolitic magma system: strontium and neodymium isotope evidence from glasses and individual phenocrysts. Geochim Cosmochim Acta 62: 3561-3574

Dawson PB, Evans JR, Iyer HM (1990) Teleseismic tomography of the compressional wave velocity structure beneath the Long Valley region, California. J Geophys Res 95: 11021-11050

Devine JD, Gardner JE, Brack HP, Layne GD, Rutherford MJ (1995) Comparison of microanalytical methods for estimating H_2O contents of silicic volcanic glasses. Am Mineral 80: 319-328

Google, TerraMetrics (2016) Long Valley caldera. Google Maps. https://www.google.com/maps/place/Long+Valley+Caldera/@37.8023694,-119.1960395,76495m/data=!3m1!1e3!4m5!3m4!1s0x8096103d4842abcb:0xe21752c39e238391!8m2!3d37.7165993!4d-118.8843024. Accessed 25 October 2016.

Halliday AN, Fallick AE, Hutchinson J, Hildreth W (1984) A Nd, Sr and O isotopic investigation into the causes of chemical and isotopic zonation in the Bishop Tuff, California. Earth Planet Sc Lett 68: 379-391

Heumann A, Davies GR (1997) Isotopic and chemical evolution of the post-caldera rhyolitic system at Long Valley, California. J Petr 38: 1661-1678

Hildreth W (2004) Volcanological perspectives on Long Valley, Mammoth Mountain, and Mono Craters: several contiguous but discrete systems. J Volcanol Geotherm Res 136: 169-198

Hildreth W, Fierstein J, Champion DE, Calvert AT (2014) Mammoth Mountain and its mafic periphery – a late Quaternary volcanic field in eastern California. Geosphere 10: 1315-1365

Hill DP, Bailey RA, Ryall AS (1985) Active tectonic and magmatic processes beneath Long Valley caldera, eastern California: an overview. J Geophys Res 90: 11111-11120

Hill DP, Prejean S (2005) Magmatic unrest beneath mammoth mountain, California. J Volcanol Geoth Res 146: 257-283

Hu Q, Smith PE, Evensen NM, York D (1994) Lasing in the Holocene: extending the $^{40}Ar/^{39}Ar$ laser probe method into the ^{14}C age range. Earth Planet Sc Lett 123: 331-336

Johnson DM, Hooper PR, Conrey RM (1999) XRF analysis of rocks and minerals for major and trace elements on a single low dilution Li-tetraborate fused bead. Adv X Ray Anal 41: 843-867

Kelleher PC (1986) The Mono Craters-Mono Lake islands volcanic complex, eastern California: evidence for several magma types, magma mixing, and a heterogeneous source region. MSc thesis, University of California Santa Cruz

Kelleher PC, Cameron KL (1990) The geochemistry of the Mono Craters-Mono Lake volcanic complex, eastern California. J Geophys Res 95: 17643-17659

Lackey JS, Valley JW, Chen JH, Stockli DF (2008) Dynamic magma systems, crustal recycling, and alteration in the Central Sierra Nevada Batholith: the oxygen isotope record. J Petr 49: 1397-1426.

Lajoie KR (1968) Late Quaternary stratigraphy and geologic history of Mono Basin, eastern California. PhD dissertation, University of California Berkeley

Marcaida M, Mangan MT, Vazquez JA, Bursik M, Lidzbarski MI (2014) Geochemical fingerprinting of Wilson Creek formation tephra layers (Mono Basin, California) using titanomagnetite compositions. J Volcanol Geoth Res 273: 1-14

Miller CD (1985) Holocene eruptions of the Inyo Volcanic Chain, California: implications for possible eruptions in Long Valley caldera. Geology 13: 14-17

Nelson ST, Montana A (1992) Sieve-textured plagioclase in volcanic rocks produced by rapid decompression. Am Mineral 77: 1242-1249

Ormerod DS (1988) Late- to post-subduction magmatic transitions in the western Great Basin, U.S.A. PhD dissertation, Open University

Pakiser LC, Press F, Kane MF (1960) Geophysical investigation of Mono Basin, California. GSA Bull 71: 415-448

Peacock JR, Mangan MT, McPhee D, Ponce DA (2015) Imaging the magmatic system of Mono Basin, California, with magnetotellurics in three dimensions. J Geophys Res: Solid Earth 120: 7273-7289

Ridolfi F, Renzulli A, Puerini M (2009) Stability and chemical equilibrium of amphibole in calc-alkaline magmas: an overview, new thermobarometric formulations and application to subduction-related volcanoes. Contrib Mineral Petr 160: 45-66

Riley P, Tikoff B, Hildreth W (2012) Transtensional deformation and structural control of contiguous but independent magmatic systems: Mono-Inyo Craters, Mammoth Mountain, and Long Valley Caldera, California. Geosphere 8: 740-751

Sampson DE, Cameron KL (1987) The geochemistry of the Inyo volcanic chain: multiple magma systems in the Long Valley region, eastern California. J Geophys

Res 92: 10403-10421

Sarna-Wojcicki AM, Lajoie KR, Meyer CE, Adam DP, Robinson SW, Anderson RS (1988) Tephrochronologic studies of sediment cores from Walker Lake, Nevada. US Geol Surv Open File Rep 88-548

Sieh KE, Bursik MI (1986) Most recent eruption of the Mono Craters, eastern Central California. J Geophys Res 91: 12539-12571

Sparks RJS, Sigurdsson H, Wilson L (1977) Magma mixing: a mechanism for triggering acid explosive eruptions. Nature 267: 315-318

Sr-Nd-Pb-U-Th isotope procedures. Isotope Geochemistry and Geochronology Research Centre. http://www.carleton.ca/iggrc/

Stine S (1987) Mono Lake: the past 4000 years. Dissertation, University of California Berkeley

Stix J, Gauthier G, Ludden JN (1995) A critical look at quantitative laser-ablation ICP-MS analysis of natural and synthetic glasses. Can Mineral 33: 435-444

Todt W, Cliff RA, Hanser A, Hoffmann AW (1996) ^{202}Pb-^{205}Pb double spike for high-precision lead isotope analysis. In: Basu A, Hart SR (eds) Earth processes: reading the isotopic code. AGU Geophysical Monograph 95. AGU, Washington, 429-437.

Van Kooten GK (1981) Pb and Sr systematics of ultrapotassic and basaltic rocks from the central Sierra Nevada, California. Contrib Mineral Petr 76: 378-385

Varga RJ, Bailey RA, Suemnicht GA (1990) Evidence for 600 year-old basalt and magma mixing at Inyo Craters volcanic chain, Long Valley caldera, California. J Geophys Res 95: 21441-21450

Vazquez JA, Lidzbarski MI (2012) High-resolution tephrochronology of the Wilson Creek Formation (Mono Lake, California) and Laschamp event using ^{238}U-^{230}Th SIMS dating of accessory mineral rims. Earth Planet Sc Lett 357-358: 54-67

Wark DA, Hildreth W, Spear FS, Cherniak DJ, Watson EB (2007) Pre-eruption recharge of the Bishop magma system. Geology 35: 235-238

White JDL (2000) Subaqueous eruption-fed density currents and their deposits. Precambrian Res 101: 87-109

Wood SH (1983) Chronology of late Pleistocene and Holocene volcanics, Long Valley and Mono Basin geothermal areas, eastern California. US Geol Surv Open File Rep 83-747

Zimmerman SR, Hemming SR, Hemming NG, Tomascak PB, Pearl C (2011) High-resolution chemostratigraphic record of late Pleistocene lake-level variability, Mono Lake, California. Geol Soc Am Bull 123: 2320-2334

Figure captions

Fig. 1a: Map of the Long Valley region, adapted from Google and TerraMetrics (2016). Boxes indicate (a) Long Valley caldera, (b) Mono domes – see Fig. 1b for further detail – and (c) Mono Lake – see Fig. 1c for further detail.

Fig. 1b: Map of the Mono domes, adapted from Kelleher and Cameron (1990). Domes are numbered using the scheme of Wood (1983).

Fig. 1c: Map of Mono Lake, adapted from Bailey (1989).

Fig. 2: Field photographs of mafic enclaves. **(a)** Elongate enclave in flow-banded rhyolite, sample BB-2011-05, Mono dome 14. **(b)** Small, rounded enclave in sparsely porphyritic rhyolite, sample BB-2011-14, North Deadman Creek dome. **(c)** Reddish, rounded enclave in porphyritic rhyolite, sample BB-2011-05, Mono dome 14. **(d)** Numerous elongate enclaves in porphyritic rhyolite, sample BB-2012-05, Mono dome 18; photo courtesy Patrick Beaudry.

Fig. 3: Field photographs of dacite lava textures in Mono Lake. **(a)** Finely layered dacite and sediment of peperite on Paoha Island, sample BB-2011-11c. **(b)** Decimeter-scale columnar jointing in the Negit islets dacite, sample BB-2011-02. **(c)** Welded ledges at the summit of the Negit Island dacitic cinder cone, reminiscent of Strombolian-style deposits, sample BB-2011-19; photo courtesy Patrick Beaudry. **(d)** Brecciated Negit islets dacite cemented by Mono Lake tufa, sample BB-2011-02.

Fig. 4: Intermediate-composition clot containing glass, biotite, and plagioclase in sample BB-2011-10, Paoha Island dacite.

Fig. 5: Plagioclase crystals with pronounced disequilibrium textures are present in all crystal-bearing lavas of the Mono Basin. **(a)** Plagioclase with sieved center and calcic overgrowth rim, sample BB-2011-05, Mono dome 14. **(b)** Partially dissolved, finely sieved plagioclase, sample BB-2011-10, Paoha Island dacite. **(c)** Finely sieved plagioclase pierced by biotite, sample BB-2011-18, Negit Island. **(d)** Coarsely sieved, zoned plagioclase, sample BB-2012-17, Mono dome 29.

Fig. 6: Intimate commingling of enclaves and host lava. **(a)** Rhyolitic inclusion within an andesitic enclave, sample BB-2011-05b-2, Mono dome 14 enclave. **(b)** Inclusions of

solidified rhyolitic magma at the enclave-host border, sample BB-2011-05b-2, Mono dome 14 enclave.

Fig. 7: **(a)** K_2O and SiO_2 show a positive correlation, except at high SiO_2 values, where K_2O declines in the Mono domes. **(b)** Rb and SiO_2 are positively correlated throughout the entire sample suite. Several of the mafic enclave analyses presented in Figs. 7-11, as well as the analysis of Mono dome 12, are from Kelleher and Cameron (1990), and an Inyo enclave sample from Glass Creek is taken from Varga et al. (1990).

Fig. 8: **(a)** K_2O and Rb show a positive correlation, except at high Rb values, where K_2O declines in the Mono domes. **(b)** P_2O_5 and Rb are negatively correlated except for the most mafic lavas. **(c)** V decreases with increasing Rb content throughout the entire system and is completely depleted in the Mono domes. **(d)** Zr concentrations increase with Rb concentration in the mafic and intermediate lavas, then decline abruptly in the more evolved lavas of the Paoha Island rhyolite, the Inyo domes, and the Mono domes.

Fig. 9: **(a-b)** Y and Nb concentrations are notably different between Paoha Island and Negit Island. They are broadly consistent within individual enclave populations. **(c-d)** LREE concentrations are depleted in the Mono domes compared to the less silicic lavas. The Mono domes form clusters at different LREE contents.

Fig. 10: The Mono Lake lavas have noticeable differences in trace element content compared to the more mafic and more felsic lavas. **(a)** Sr concentrations in Mono Lake samples show some overlap with more mafic enclaves and lavas and are enriched relative to the Mono domes. **(b)** The Mono Lake lavas are extremely enriched in Ba compared to all other samples.

Fig. 11: **(a-b)** The mafic lavas of the Mono Basin have the least radiogenic Sr and Nd values of the Long Valley Volcanic Field. The Negit Island lavas tend toward more crustal values than the Paoha Island lavas, and the lavas of both islands are more radiogenic than the Mono dome rhyolites. **(c-d)** Crustal signatures dominate O isotope values throughout the Mono Basin. This is the case even in the otherwise mantle-like mafic magmas. Regional isotopic data used in plotting fields come from Van Kooten (1981); Halliday et al. (1984); Chaudet (1986); Kelleher (1986); Ormerod (1986); Sampson and Cameron (1987); Christensen and DePaolo (1993); Cousens (1996); Heumann and Davies (1997); Davies and Halliday (1998); and Bailey (2004) (Online Resource 1).

Fig. 12: Lavas throughout the Mono Basin exhibit multiple glass populations. **(a-b)** Paoha Island has clots of material that is more mafic (higher CaO, lower K_2O) than the host dacite. **(c-d)** Inclusions of glass in the Mono domes are basaltic in composition; rhyolitic inclusions in the Mono dome andesitic enclaves have glass that is more felsic (lower CaO, higher K_2O) than the andesite.

Fig. 13: Two distinct populations of amphiboles characterize the Mono Lake lavas versus the Inyo domes. **(a)** The Mono Lake population has noticeably lower Si and Fe compared to the Inyo population, and formed at **(b)** generally higher temperatures and pressures than the Inyo population.

Figure 1a

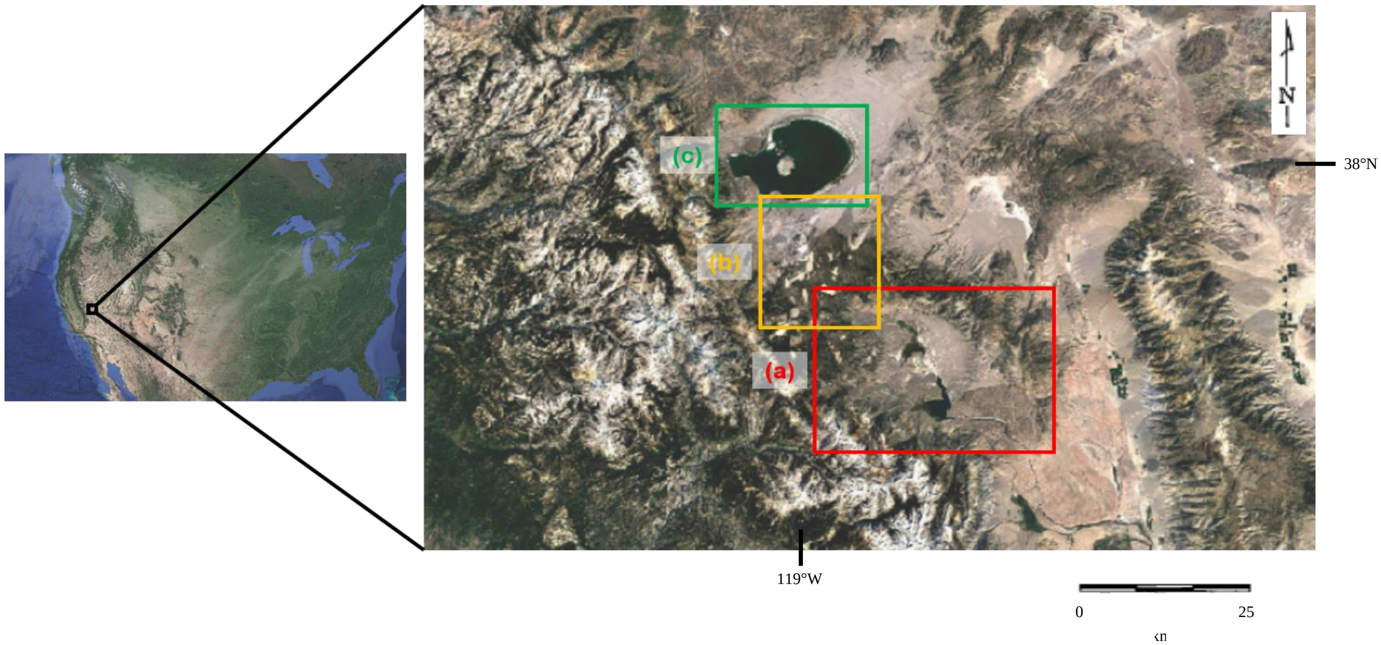

Figure 1b

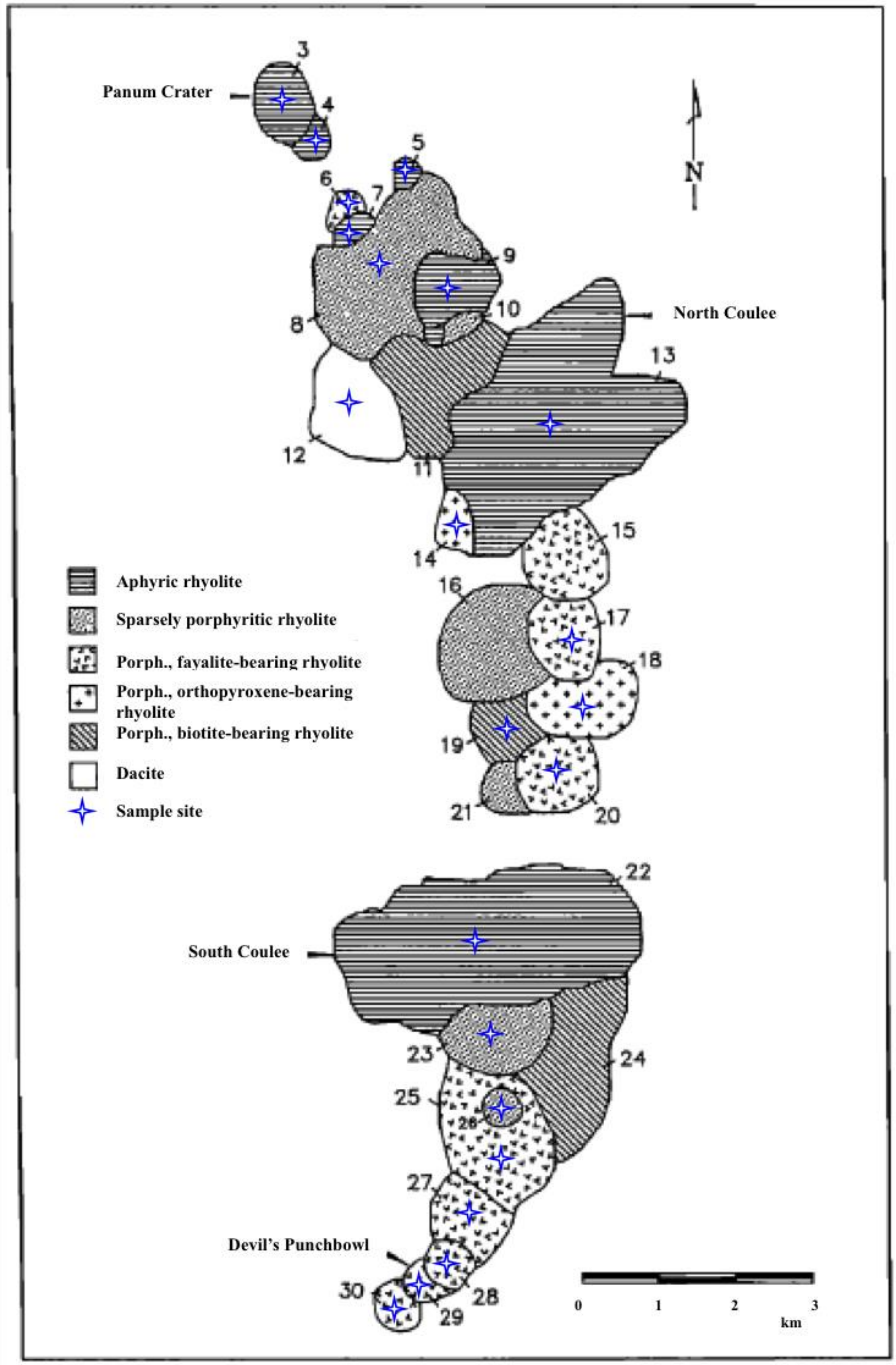

3
Panum Crater
4
5
6
7
N
9
8
10
North Coulee
13
12
11
14
15
16
17
18
19
20
21
Aphyric rhyolite
Sparsely porphyritic rhyolite
Porph., fayalite-bearing rhyolite
Porph., orthopyroxene-bearing rhyolite
Porph., biotite-bearing rhyolite
Dacite
Sample site
22
South Coulee
23
24
25
26
27
Devil's Punchbowl
28
29
30
0
1
2
3
km

Figure 1c


N
Black Point
Negit islets
Negit
Island
Paoha
Island
Sample site
Paoha Island
Negit Island
Mono Lake rhyolite
Basalt
Mono Lake shoreline
0 1 2 3
km

Figure 2

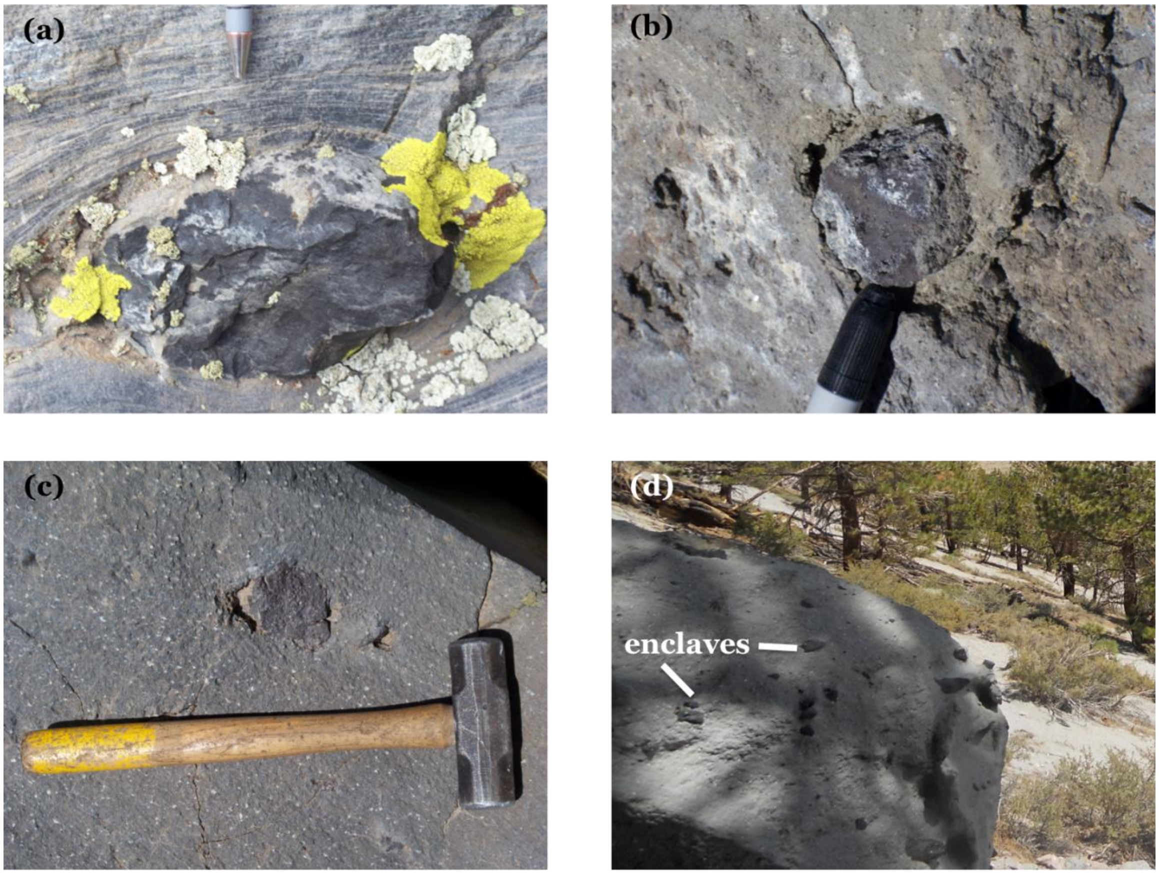

Figure 3

Figure 4

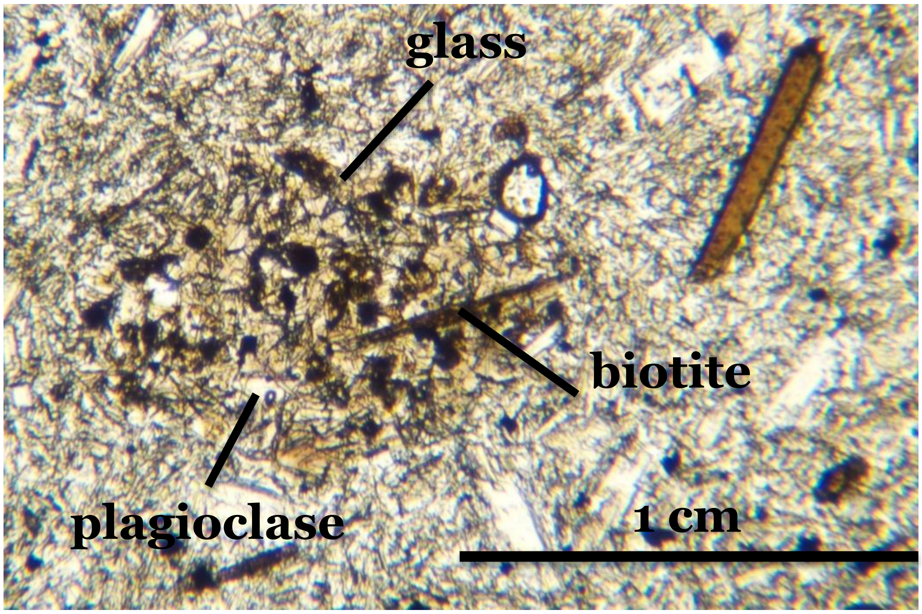

Figure 5

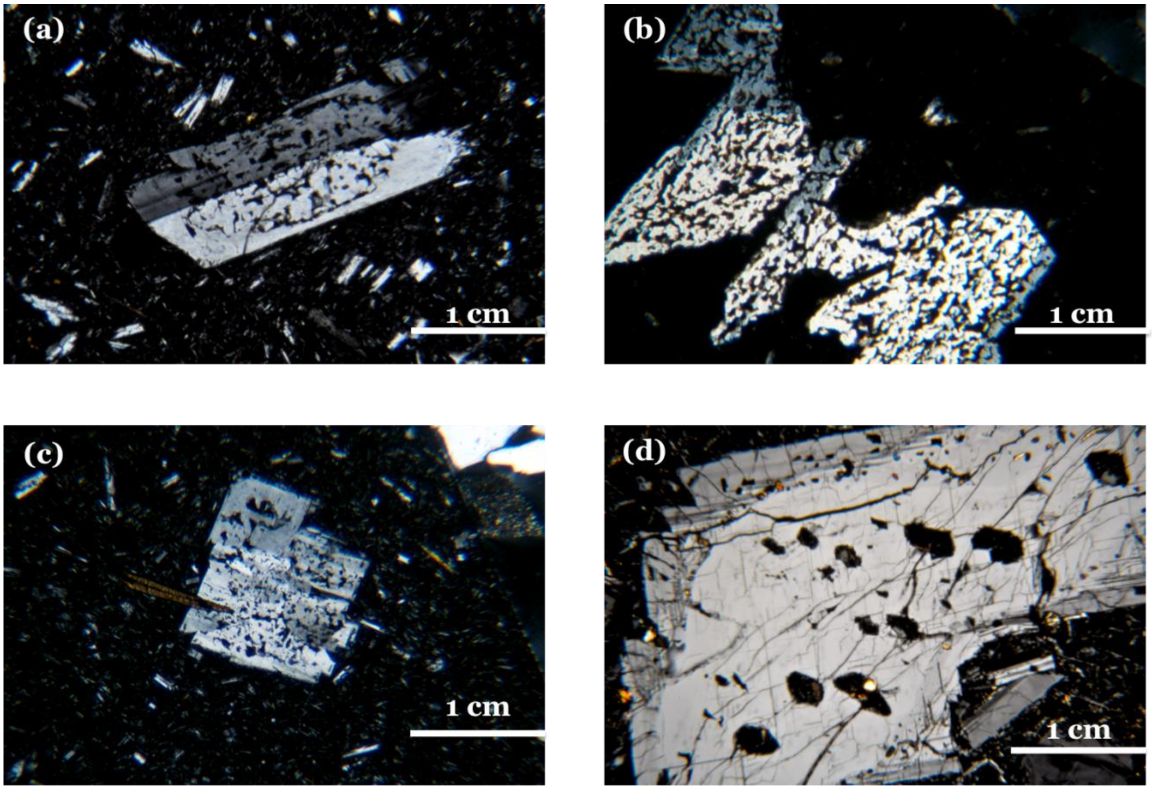

Figure 6

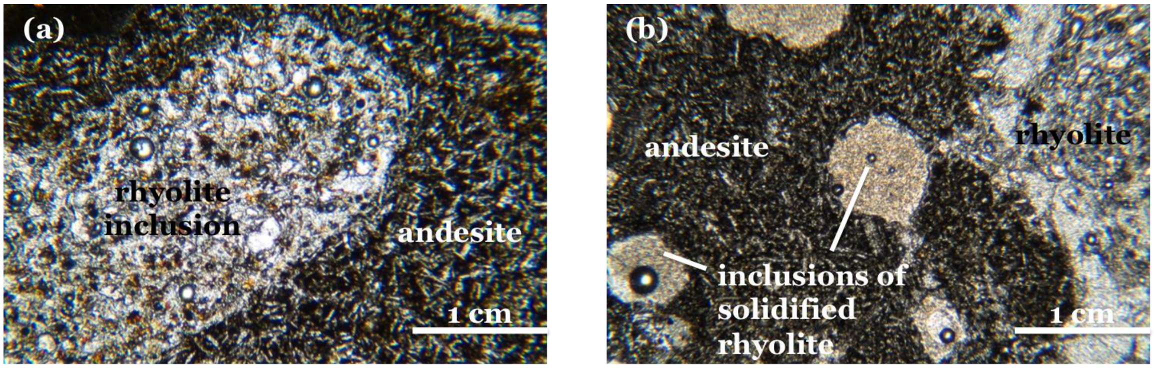
(a)
rhyolite inclusion
andesite
1 cm
(b)
andesite
rhyolite
inclusions of solidified rhyolite
1 cm

Figure 7

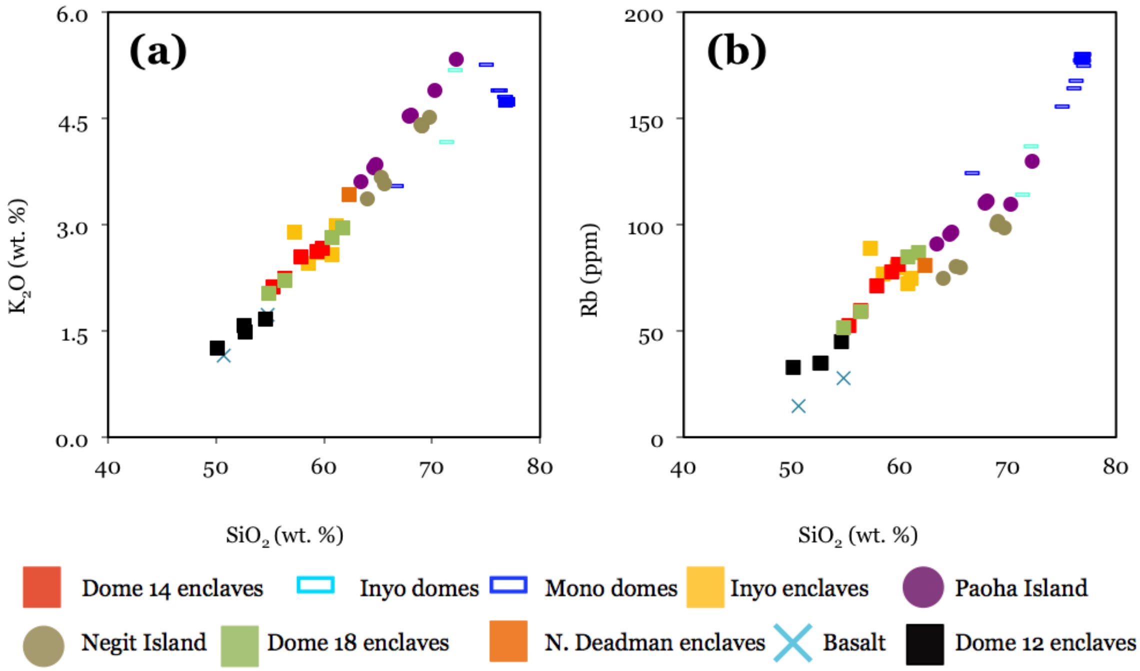
(a)
6.0
4.5
3.0
1.5
0.0
40
50
60
70
80
K_2O (wt. %)
SiO_2 (wt. %)
(b)
200
150
100
50
0
40
50
60
70
80
Rb (ppm)
SiO_2 (wt. %)
Dome 14 enclaves
Inyo domes
Mono domes
Inyo enclaves
Paoha Island
Negit Island
Dome 18 enclaves
N. Deadman enclaves
Basalt
Dome 12 enclaves

Figure 8

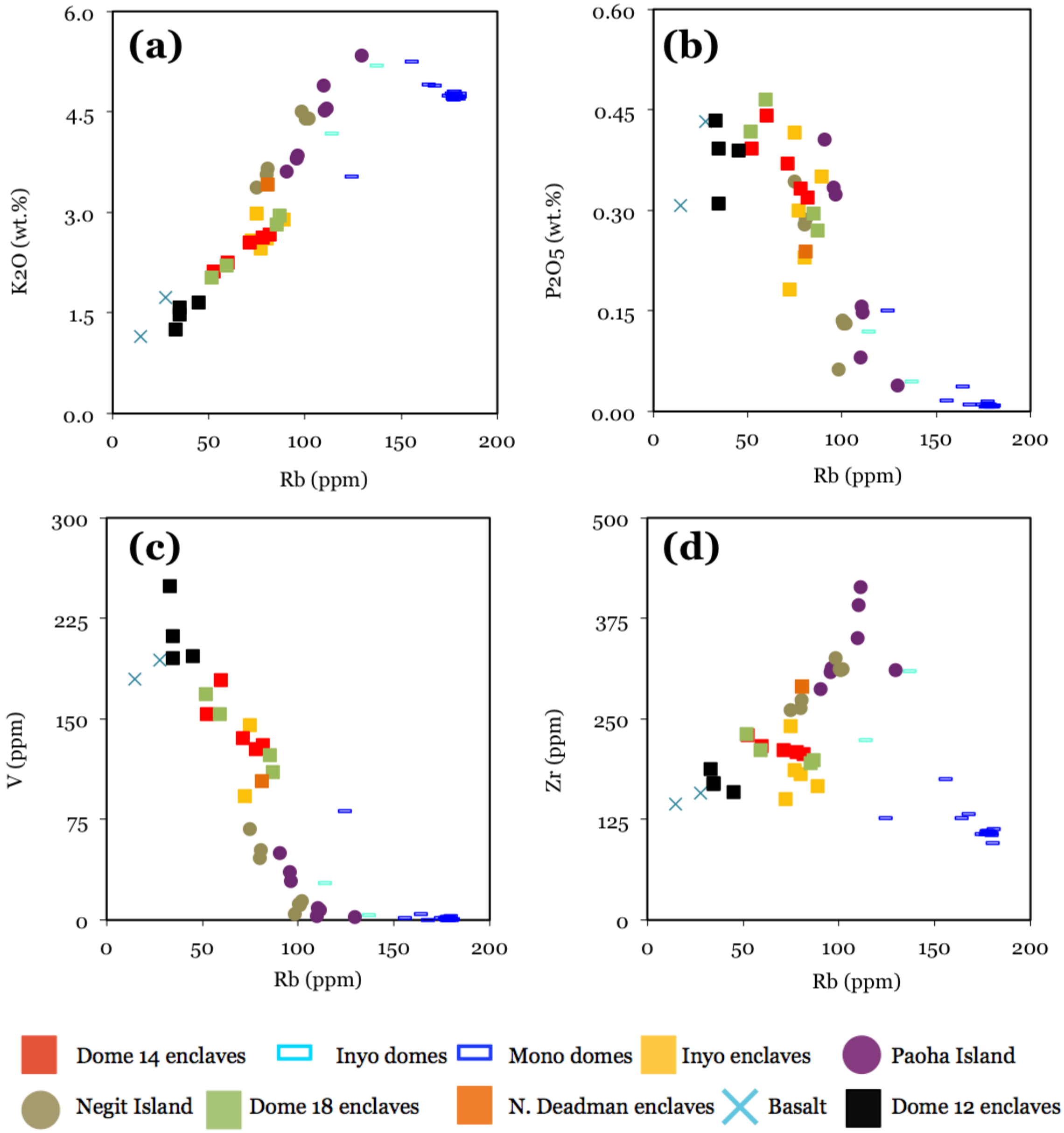
(a)
K2O (wt.%)
6.0
4.5
3.0
1.5
0.0
0
50
100
150
200
Rb (ppm)
(b)
P2O5 (wt.%)
0.60
0.45
0.30
0.15
0.00
0
50
100
150
200
Rb (ppm)
(c)
V (ppm)
300
225
150
75
0
0
50
100
150
200
Rb (ppm)
(d)
Zr (ppm)
500
375
250
125
0
0
50
100
150
200
Rb (ppm)
Dome 14 enclaves
Inyo domes
Mono domes
Inyo enclaves
Paoha Island
Negit Island
Dome 18 enclaves
N. Deadman enclaves
Basalt
Dome 12 enclaves

Figure 9

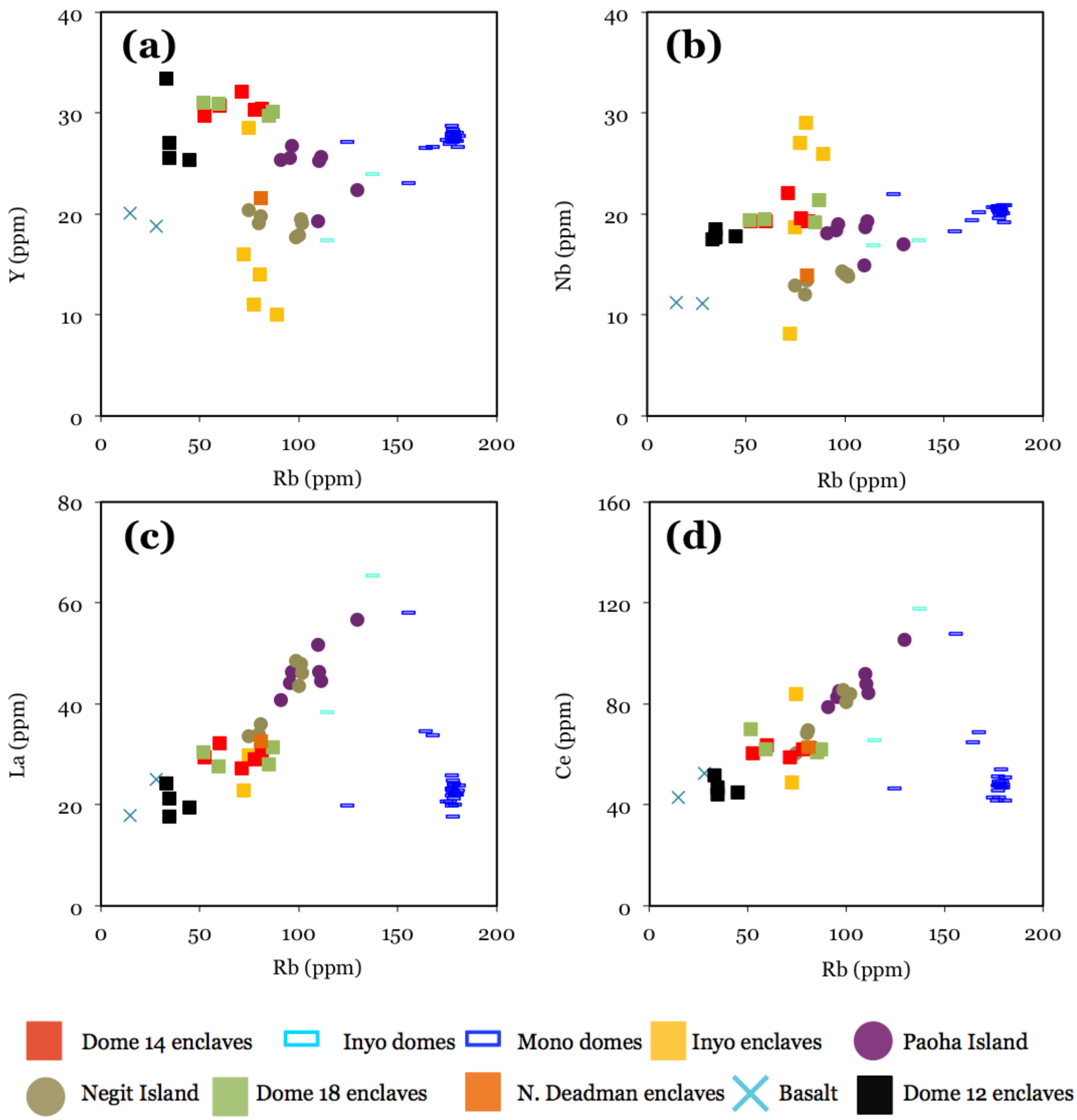
(a)
Y (ppm)
Rb (ppm)
(b)
Nb (ppm)
Rb (ppm)
(c)
La (ppm)
Rb (ppm)
(d)
Ce (ppm)
Rb (ppm)
Dome 14 enclaves
Inyo domes
Mono domes
Inyo enclaves
Paoha Island
Negit Island
Dome 18 enclaves
N. Deadman enclaves
Basalt
Dome 12 enclaves

Figure 10

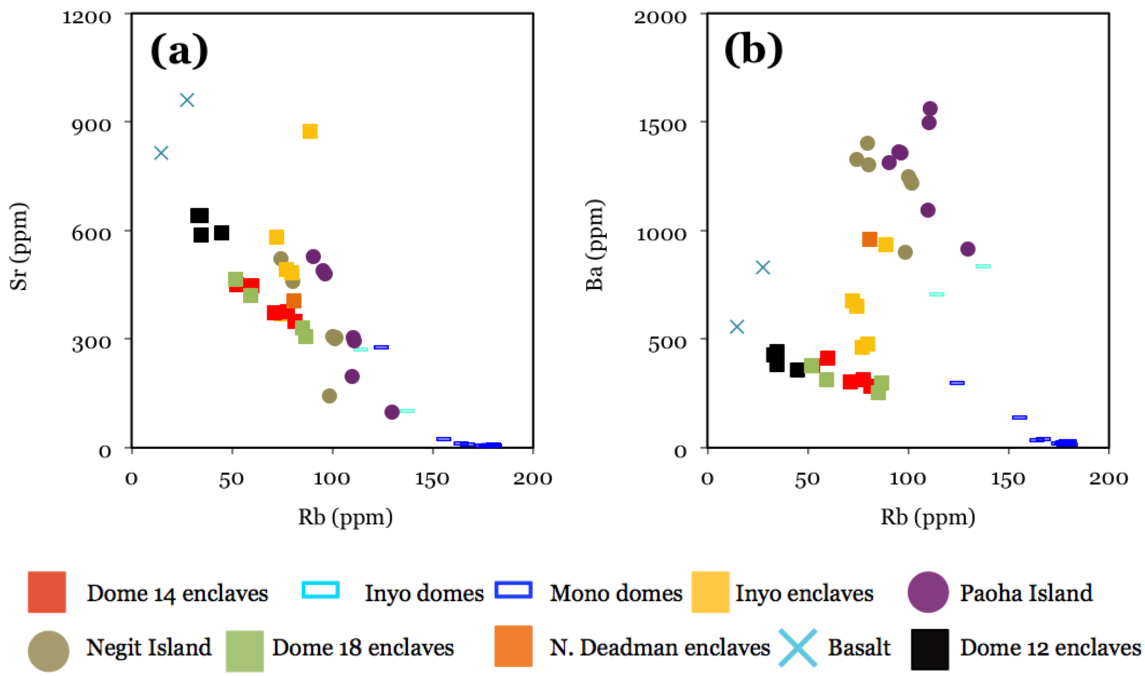

(a)
(b)
1200
900
600
300
0
2000
1500
1000
500
0
50
100
150
200
Sr (ppm)
Ba (ppm)
Rb (ppm)
Rb (ppm)
Dome 14 enclaves
Inyo domes
Mono domes
Inyo enclaves
Paoha Island
Negit Island
Dome 18 enclaves
N. Deadman enclaves
Basalt
Dome 12 enclaves

Figure 11

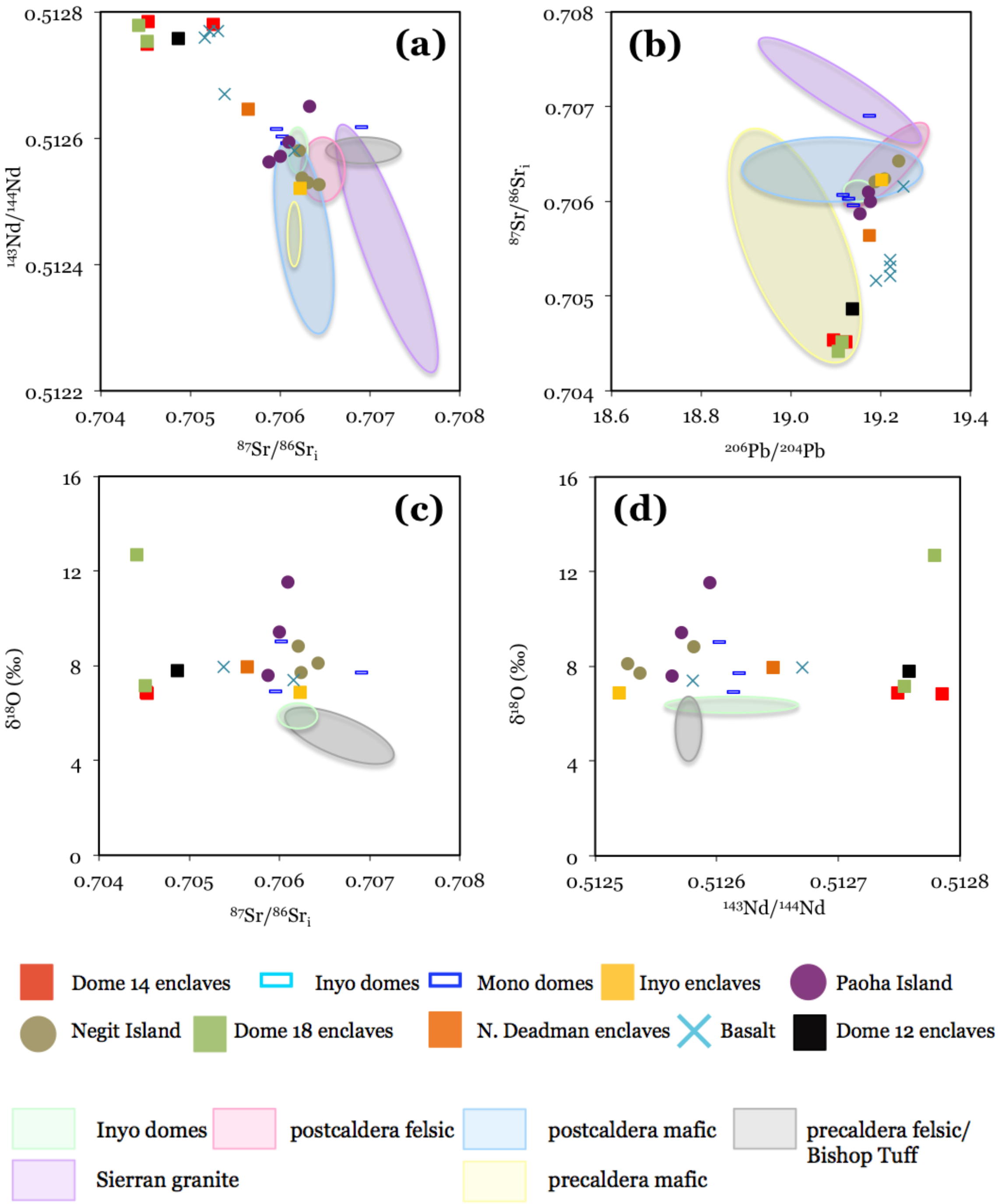
(a)
0.5128
0.5126
0.5124
0.5122
^{143}Nd/^{144}Nd
0.704
0.705
0.706
0.707
0.708
^{87}Sr/^{86}Sr$_i$
(b)
0.708
0.707
0.706
0.705
0.704
^{87}Sr/^{86}Sr$_i$
18.6
18.8
19.0
19.2
19.4
^{206}Pb/^{204}Pb
(c)
16
12
8
4
0
δ^{18}O (‰)
0.704
0.705
0.706
0.707
0.708
^{87}Sr/^{86}Sr$_i$
(d)
16
12
8
4
0
δ^{18}O (‰)
0.5125
0.5126
0.5127
0.5128
^{143}Nd/^{144}Nd
Dome 14 enclaves
Inyo domes
Mono domes
Inyo enclaves
Paoha Island
Negit Island
Dome 18 enclaves
N. Deadman enclaves
Basalt
Dome 12 enclaves
Inyo domes
postcaldera felsic
postcaldera mafic
precaldera felsic/ Bishop Tuff
Sierran granite
precaldera mafic

Figure 12

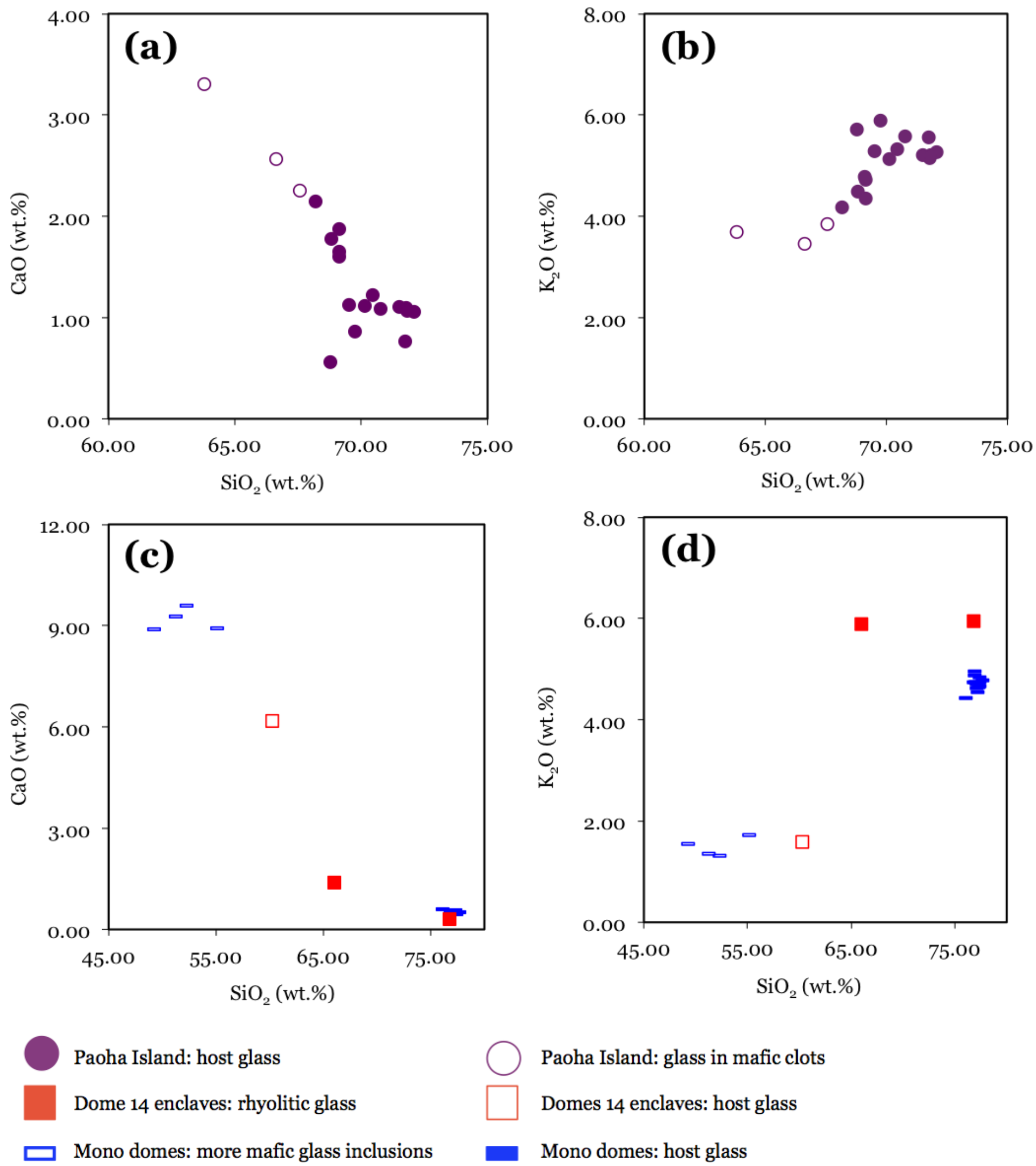

(a)
(b)
(c)
(d)
CaO (wt.%)
K_2O (wt.%)
SiO_2 (wt.%)
4.00
3.00
2.00
1.00
0.00
8.00
6.00
4.00
2.00
0.00
12.00
9.00
6.00
3.00
0.00
60.00
65.00
70.00
75.00
45.00
55.00
65.00
75.00
Paoha Island: host glass
Paoha Island: glass in mafic clots
Dome 14 enclaves: rhyolitic glass
Domes 14 enclaves: host glass
Mono domes: more mafic glass inclusions
Mono domes: host glass

Figure 13

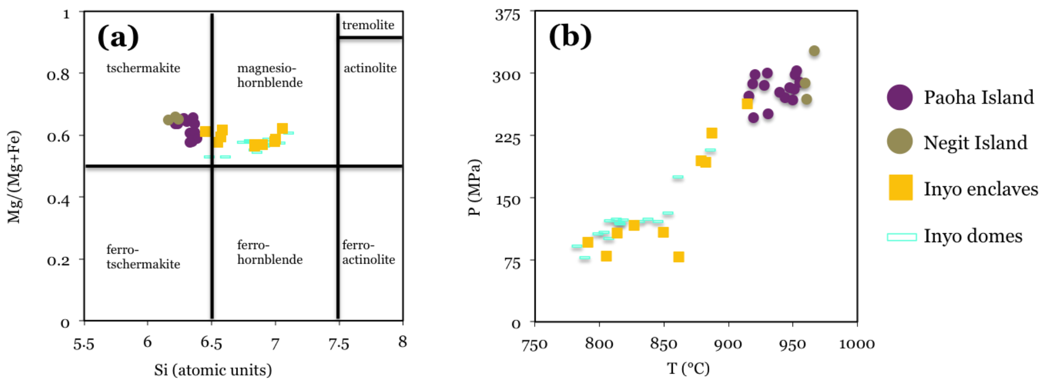

(a)
tschermakite
magnesio-hornblende
tremolite
actinolite
ferro-tschermakite
ferro-hornblende
ferro-actinolite
Mg/(Mg+Fe)
Si (atomic units)
(b)
P (MPa)
T (°C)
Paoha Island
Negit Island
Inyo enclaves
Inyo domes

Table 1: Mono Basin samples from the 2011 and 2012 field seasons.

Sample Number	Magma group	Coordinates	Locality	Rock type
BB-2011-01	Negit Island	11S 0321345/4211192	Norway Island	sparsely porphyritic rhyolite
BB-2011-02	Negit Island	11S 0320829/4211181	Tahiti Island	sparsely porphyritic, flow banded dacite
BB-2011-03	Negit Island	11S 0320985/4211108	Tahiti Island	sparsely porphyritic, flow banded dacite
BB-2011-04	Mono domes	11S 0322636/4195314	Mono dome 13 (North Coulée)	aphyric rhyolite
BB-2011-04b	Mono domes	11S 0322377/4195303	Mono dome 13 (North Coulée)	breccia
BB-2011-05	Mono domes	11S 0322199/4195444	Mono dome 14	orthopyroxene- and enclave-bearing rhyolite
BB-2011-05b	Dome 14 enclaves	11S 0322199/4195444	Mono dome 14	mafic enclaves
BB-2011-06	Mono domes	11S 0321305/4196207	Mono dome 12	enclave-bearing dacite
BB-2011-07	Mono domes	11S 0320836/4198805	Mono dome 6	fayalite-bearing rhyolite
BB-2011-08	Mono domes	11S 0321078/4198661	Mono dome 7	aphyric rhyolite
BB-2011-09	Paoha Island	11S 0322513/4207227	Paoha Island (east dacite flow)	peperite
BB-2011-10	Paoha Island	11S 0322569/4207300	Paoha Island (east dacite flow)	sparsely porphyritic dacite
BB-2011-11	Paoha Island	11S 0322287/4207052	Paoha Island (east dacite flow)	grey dacite in peperite
BB-2011-11b	Paoha Island	11S 0322287/4207052	Paoha Island (east dacite flow)	black dacite in peperite
BB-2011-11c	Paoha Island	11S 0322287/4207052	Paoha Island (east dacite flow)	peperite
BB-2011-12	Paoha Island	11S 0322458/4208935	Paoha Island (northeast cinder cones)	sparsely porphyritic dacite
BB-2011-12b	Paoha Island	11S 0322458/4208935	Paoha Island (northeast cinder cones)	dacitic scoria
BB-2011-13	Paoha Island	11S 0322273/4209031	Paoha Island (northeast cinder cones)	dacitic bomb

Table 1
(continued)

Sample Number	Magma group	Coordinates	Locality	Rock type
BB-2011-14	Mono domes	11S 0321591/4176223	North Deadman Creek Dome	enclave-bearing rhyolite
BB-2011-14b	N. Deadman Creek enclaves	11S 0321591/4176223	North Deadman Creek Dome	mafic enclaves
BB-2011-15	Inyo domes	11S 0322210/4176138	South Deadman Creek Dome	coarse-grained rhyolite
BB-2011-15b	Inyo domes	11S 0322210/4176138	South Deadman Creek Dome	fine-grained rhyolite
BB-2011-15c	Inyo enclaves	11S 0322210/4176138	South Deadman Creek Dome	mafic enclaves
BB-2011-16	Paoha Island	11S 0321501/4209348	Paoha Island (Lunacy Point)	sparsely porphyritic dacite
BB-2011-17	Paoha Island	11S 0320844/4208752	Paoha Island (west rhyolite flow)	sparsely porphyritic rhyolite
BB-2011-18	Negit Island	11S 0320116/4209814	Negit Island (east dacite flow)	sparsely porphyritic dacite
BB-2011-19	Negit Island	11S 0319934/4209903	Negit Island (cinder cone)	dacitic scoria
BB-2011-20	Mono domes	11S 0321937/4183577	Wilson Butte	sparsely porphyritic rhyolite
BB-2011-20b	-	11S 0321937/4183577	Wilson Butte	xenoliths
BB-2011-21	Basalt	11S 0318272/4185971	June Lake cinder cone	oxidized vent breccia
BB-2011-22	Basalt	11S 0318310/4188377	June Lake basalt	basalt
BB-2011-23	Negit Island	11S 0314795/4205740	Mono Lake shoreline	pumice
BB-2011-24	Basalt	11S 0315244/4210530	Black Point	degassed basalt
BB-2011-24b	-	11S 0315244/4210530	Black Point	vesicular basalt

Table 1
(continued)

Sample Number	Magma group	Coordinates	Locality	Rock type
BB-2011-24c	-	11S 0315244/4210530	Black Point	pumices
BB-2011-24d	-	11S 0315244/4210530	Black Point	sedimentary matrix
BB-2011-24e	-	11S 0315244/4210530	Black Point	fine, sandy layer
BB-2012-01	-	11S 0345948/4180113	Glass Mountain	rhyolite
BB-2012-01b	-	11S 0345948/4180113	Glass Mountain	xenoliths
BB-2012-02	Mono domes	11S 0322262/4195540	Mono dome 14	orthopyroxene- and enclave-bearing rhyolite
BB-2012-02b	Dome 14 enclaves	11S 0322262/4195540	Mono dome 14	mafic enclaves
BB-2012-03	Mono domes	11S 0321340/4196196	Mono dome 12	enclave-bearing dacite
BB-2012-03b	Dome 12 enclaves	11S 0321340/4196196	Mono dome 12	mafic enclaves
BB-2012-04	Mono domes	11S 0321865/4176572	North Deadman Creek Dome	enclave-bearing rhyolite
BB-2012-04b	N. Deadman Creek enclaves	11S 0321865/4176572	North Deadman Creek Dome	mafic enclaves
BB-2012-05	Mono domes	-	Mono dome 18	orthopyroxene- and enclave-bearing rhyolite
BB-2012-05b	Dome 18 enclaves	-	Mono dome 18	mafic enclaves
BB-2012-06	Mono domes	11S 0320260/4199922	Mono dome 3	aphyric rhyolite
BB-2012-06b	Mono domes	11S 0320260/4199922	Mono dome 3	breadcrust bomb
BB-2012-06c	Mono domes	11S 0320260/4199922	Mono dome 3	obsidian

Table 1
(continued)

Sample Number	Magma group	Coordinates	Locality	Rock type
BB-2012-07	Mono domes	11S 0320485/4199437	Mono dome 4	aphyric rhyolite
BB-2012-08	Mono domes	11S 0321801/4183976	Wilson Butte	sparsely porphyritic rhyolite
BB-2012-08b	-	11S 0321801/4183976	Wilson Butte	xenoliths
BB-2012-09	-	11S 0342840/4179773	Intracaldera dacite dome	porphyritic dacite
BB-2012-09b	-	11S 0342840/4179773	Intracaldera dacite dome	columnar dacite
BB-2012-10	Mono domes	11S 0321639/4199224	Mono dome 5	aphyric rhyolite
BB-2012-11	Mono domes	11S 0323738/4190283	Mono dome 22 (South Coulée)	aphyric rhyolite
BB-2012-11b	Mono domes	11S 0323738/4190283	Mono dome 22 (South Coulée)	obsidian
BB-2012-11c	Mono domes	11S 0323738/4190283	Mono dome 22 (South Coulée)	pumice
BB-2012-12	Paoha Island	11S 0322289/4207031	Paoha Island (east dacite flow)	peperite sediment layer
BB-2012-12b	Paoha Island	11S 0322289/4207031	Paoha Island (east dacite flow)	peperite dacite inclusions in sediment layer
BB-2012-12c	Paoha Island	11S 0322289/4207031	Paoha Island (east dacite flow)	peperite dacite layer
BB-2012-13	Paoha Island	11S 0322311/4207325	Paoha Island (eastern shoreline)	Paoha Island sediment
BB-2012-14	Negit Island	11S 0320302/4210218	Negit Island (north dacite flow)	sparsely porphyritic dacite
BB-2012-14b	Negit Island	11S 0320302/4210218	Negit Island (north dacite flow)	sparsely porphyritic dacite
BB-2012-15	Negit Island	11S 0320043/4209970	Negit Island (cinder cone)	sparsely porphyritic dacite

Table 1
(continued)

Sample Number	Magma group	Coordinates	Locality	Rock type
BB-2012-15b	Negit Island	11S 0320043/4209970	Negit Island (cinder cone)	dacitic bombs
BB-2012-16	Mono domes	11S 0321147/4187050	Mono dome 30	fayalite-bearingrhyolite
BB-2012-17	Mono domes	11S 0321604/4187195	Mono dome 29	fayalite-bearingrhyolite
BB-2012-18	Mono domes	11S 0321796/4187441	Mono dome 28	fayalite-bearing rhyolite
BB-2012-18b	-	11S 0321796/4187441	Mono dome 28	xenoliths
BB-2012-19	Mono domes	11S 0322473/4187760	Mono dome 27	fayalite-bearing rhyolite
BB-2012-20	Mono domes	11S 0322947/4189213	Mono dome 25	fayalite-bearing rhyolite
BB-2012-21	Mono domes	11S 0322681/4189219	Mono dome 26	sparsely porphyritic rhyolite
BB-2012-21b	-	11S 0322681/4189219	Mono dome 26	xenoliths
BB-2012-22	Mono domes	11S 0323162/4189746	Mono dome 23	sparsely porphyritic rhyolite
BB-2012-23	Mono domes	11S 0322531/4198256	Mono dome 9	sparsely porphyritic rhyolite
BB-2012-24	Mono domes	11S 0322299/4198350	Mono dome 8	aphyric rhyolite
BB-2012-25	Mono domes	11S 0323560/4192222	Mono dome 20	fayalite-bearing rhyolite
BB-2012-26	Mono domes	11S 0322608/4193567	Mono dome 19	biotite-bearing rhyolite
BB-2012-27	Mono domes	11S 0323467/4193790	Mono dome 17	fayalite-bearing rhyolite
BB-2012-27b	-	11S 0323467/4193790	Mono dome 17	xenoliths

Table 2

Table 2: Major and trace element compositions of the Mono Basin lavas. Major elements reported in wt.%. Trace elements reported in ppm. Blank space indicates element below the detection limit of the XRF.

Sample	BB-2011-04	BB-2011-05	BB-2011-07	BB-2011-08	BB-2011-14	BB-2011-20	BB-2012-05
Magma group	Mono dome 13	Mono dome 14	Mono dome 6	Mono dome 7	Mono domes (N. Dmn. Crk.)	Mono domes (Wlsn. Bt.)	Mono dome 18
UTM	11S 0322636/4195 314	11S 0322199/4195 444	11S 0320836/4198 805	11S 0321078/4198 661	11S 0321591/4176 223	11S 0321937/4183 577	
SiO_2	75.83	74.49	74.33	76.06	73.10	75.80	73.48
TiO_2	0.06	0.07	0.06	0.06	0.11	0.06	0.07
Al_2O_3	12.46	12.57	12.21	12.48	13.13	12.43	12.43
FeO_T	1.04	1.13	0.98	1.02	1.27	1.02	1.13
MnO	0.04	0.05	0.04	0.04	0.05	0.04	0.05
MgO	0.01	0.02	0.00	0.00	0.05	0.00	0.06
CaO	0.54	0.57	0.51	0.54	0.64	0.53	0.69
Na_2O	3.97	3.93	3.81	3.96	3.91	3.96	3.81
K_2O	4.65	4.78	4.58	4.64	5.12	4.63	4.73
P_2O_5	0.01	0.01	0.01	0.01	0.02	0.01	0.04
Total	98.62	97.61	96.54	98.80	97.39	98.49	96.49
Ba	28	41	20	23	137	22	37
Ce	47	69	43	48	108	48	65
Cr	3	2	3	3	4	4	3
Cu	1	2	2	2	1	1	4
Ga	17	18	17	17	16	17	17
La	24	34	21	20	58	22	35
Nb	21	20	21	21	18	21	19
Nd	19	26	20	20	38	20	25
Ni	3	3	2	4	3	2	0
Pb	28	28	29	29	28	29	27
Rb	178	168	175	177	156	180	164
Sc	2	2	2	3	2	2	3
Sr	6	9	6	7	25	6	12
Th	20	21	20	21	21	19	20
U	6	6	6	5	5	7	6
V	0	0	2	1	1	2	4
Y	28	27	27	29	23	28	27
Zn	40	43	41	41	41	41	42
Zr	111	132	107	107	175	109	126

Table 2
(continued)

Sample	BB-2012-06c	BB-2012-07	BB-2012-10	BB-2012-11b	BB-2012-16	BB-2012-17	BB-2012-18
Magma group	Mono dome 3	Mono dome 4	Mono dome 5	Mono dome 22	Mono dome 30	Mono dome 29	Mono dome 28
UTM	11S 0320260/4199922	11S 0320485/4199437	11S 0321639/4199224	11S 0323738/4190283	11S 0321147/4187050	11S 0321604/4187195	11S 0321796/4187441
SiO_2	76.11	75.89	75.62	76.08	75.36	74.76	75.15
TiO_2	0.06	0.06	0.06	0.06	0.06	0.06	0.06
Al_2O_3	12.54	12.48	12.46	12.56	12.47	12.43	12.54
FeO_T	1.03	1.03	1.02	1.02	1.01	0.97	1.02
MnO	0.05	0.05	0.04	0.05	0.05	0.04	0.05
MgO	0.01	0.00	0.00	0.00	0.01	0.01	0.00
CaO	0.53	0.54	0.54	0.54	0.53	0.54	0.54
Na_2O	3.98	3.98	3.94	3.98	3.92	3.86	3.92
K_2O	4.68	4.64	4.64	4.66	4.62	4.64	4.71
P_2O_5	0.01	0.01	0.01	0.01	0.01	0.01	0.01
Total	99.00	98.68	98.34	98.95	98.05	97.32	97.99
Ba	22	23	24	22	20	18	20
Ce	50	51	48	48	48	42	46
Cr	3	4	4	4	3	2	4
Cu	1	6	3	1	3	3	6
Ga	16	18	18	17	19	17	17
La	22	22	25	21	23	21	26
Nb	20	21	20	21	20	21	21
Nd	22	21	22	20	19	17	20
Ni	1	1	0	0	1	0	1
Pb	29	28	28	28	30	28	29
Rb	179	177	178	178	177	176	177
Sc	3	3	3	3	2	2	2
Sr	6	6	6	6	5	6	7
Th	21	20	21	21	21	20	21
U	6	7	7	6	6	5	6
V	0	1	0	2	1	1	1
Y	28	28	27	27	28	27	28
Zn	41	40	39	40	41	41	40
Zr	108	107	108	107	110	107	109

Table 2
(continued)

Sample	BB-2012-19	BB-2012-20	BB-2012-21	BB-2012-22	BB-2012-23	BB-2012-24	BB-2012-25
Magma group	Mono dome 27	Mono dome 25	Mono dome 26	Mono dome 23	Mono dome 9	Mono dome 8	Mono dome 20
UTM	11S 0322473/4187760	11S 0322947/4189213	11S 0322681/4189219	11S 0323162/4189746	11S 0322531/4198256	11S 0322299/4198350	11S 0323560/4192222
SiO_2	74.93	76.05	76.08	75.73	76.35	75.18	75.71
TiO_2	0.06	0.06	0.06	0.06	0.06	0.06	0.06
Al_2O_3	12.38	12.59	12.50	12.46	12.57	12.45	12.53
FeO_T	1.02	1.07	1.04	1.03	1.04	1.03	1.04
MnO	0.05	0.05	0.05	0.05	0.05	0.04	0.05
MgO	0.00	0.07	0.02	0.01	0.01	0.01	0.01
CaO	0.54	0.60	0.54	0.53	0.54	0.53	0.53
Na_2O	3.88	3.94	3.97	3.92	4.00	3.88	3.94
K_2O	4.68	4.65	4.68	4.68	4.69	4.67	4.65
P_2O_5	0.01	0.01	0.01	0.01	0.01	0.01	0.01
Total	97.54	99.07	98.93	98.47	99.30	97.88	98.53
Ba	19	17	20	21	23	26	19
Ce	49	43	47	48	54	49	47
Cr	4	4	2	4	4	4	3
Cu	4	4	3	3	2	3	3
Ga	17	18	18	18	18	17	18
La	23	18	22	24	22	23	20
Nb	20	21	20	20	20	21	21
Nd	22	19	21	22	25	20	22
Ni	1	3	1	1	1	1	1
Pb	29	28	29	29	29	28	29
Rb	178	178	180	178	179	177	179
Sc	3	2	2	3	3	2	3
Sr	6	5	5	6	5	6	5
Th	20	20	21	21	20	21	20
U	5	7	7	6	7	7	7
V	2	2	3	0	0	2	2
Y	28	27	27	27	28	27	27
Zn	42	39	41	42	40	40	42
Zr	110	110	106	106	107	108	109

Table 2
(continued)

Sample	BB-2012-26	BB-2012-27	M12-1A[2]	BB-2011-15	BB-2011-15b	BB-2011-22	BB-2011-24
Magma group	Mono dome 19	Mono dome 17	Mono dome 12	Inyo domes	Inyo domes	Basalt	Basalt
UTM	11S 0322608/4193 567	11S 0323467/4193 790		11S 0322210/4176 138	11S 0322210/4176 138	11S 0318310/4188 377	11S 0315244/4210 530
SiO_2	74.57	75.82	66.67	70.73	71.22	54.00	50.54
TiO_2	0.06	0.06	0.84	0.42	0.21	1.48	1.50
Al_2O_3	12.31	12.52	14.86	14.56	14.55	17.71	18.77
FeO_T	0.97	1.05	4.59	2.30	1.91	7.44	8.56
MnO	0.05	0.05		0.06	0.06	0.12	0.14
MgO	0.00	0.00	1.99	0.68	0.18	3.94	6.23
CaO	0.57	0.54	3.52	1.85	0.96	8.23	8.62
Na_2O	3.73	3.98	3.68	4.32	4.51	3.59	3.95
K_2O	4.63	4.66	3.54	4.14	5.12	1.71	1.14
P_2O_5	0.01	0.01	0.15	0.12	0.04	0.43	0.31
Total	96.91	98.68	99.84	99.19	98.75	98.65	99.76
Ba	29	15	297	708	835	829	559
Ce	42	51	47	66	118	52	43
Cr	3	3	14	5	4	28	21
Cu	3	3		3	2	24	25
Ga	17	17		18	18	20	19
La	23	24	20	38	65	25	18
Nb	19	21	22	17	17	11	11
Nd	17	21	18	23	39	25	21
Ni	2	3	15	5	4	17	62
Pb	29	28		26	25	10	5
Rb	180	181	124	114	137	28	15
Sc	2	1	9	4	4	20	20
Sr	10	5	277	273	103	961	816
Th	21	21		13	17	3	3
U	6	7		4	5	1	1
V	0	1	82	28	4	194	180
Y	27	28	27	17	24	19	20
Zn	38	42		50	54	80	83
Zr	96	113	126	224	310	157	144

Table 2
(continued)

Sample	BB-2011-09	BB-2011-10	BB-2011-11	BB-2011-12	BB-2011-13	BB-2011-16	BB-2011-17
Magma group	Paoha Island	Paoha Island	Paoha Island	Paoha Island	Paoha Island	Paoha Island	Paoha Island
UTM	11S 0322513/4207227	11S 0322569/4207300	11S 0322287/4207052	11S 0322458/4208935	11S 0322273/4209031	11S 0321501/4209348	11S 0320844/4208752
SiO_2	66.22	67.27	69.56	64.56	63.26	64.52	68.99
TiO_2	0.54	0.53	0.17	0.93	1.05	0.90	0.29
Al_2O_3	15.76	15.90	14.38	16.53	16.63	16.47	15.24
FeO_T	2.95	2.90	1.88	4.39	4.88	4.25	2.36
MnO	0.07	0.07	0.06	0.09	0.10	0.09	0.07
MgO	0.65	0.62	0.15	1.28	1.52	1.22	0.31
CaO	1.87	1.82	0.90	3.14	3.51	3.05	1.40
Na_2O	4.86	5.04	4.05	4.93	4.79	4.93	4.64
K_2O	4.41	4.50	5.14	3.80	3.60	3.83	4.81
P_2O_5	0.15	0.15	0.04	0.33	0.40	0.32	0.08
Total	97.51	98.79	96.34	99.98	99.74	99.60	98.18
Ba	1498	1560	917	1362	1315	1358	1094
Ce	88	84	105	83	79	85	92
Cr	3	3	4	2	3	2	3
Cu	1	1	1	2	14	1	2
Ga	21	21	17	22	21	21	20
La	46	45	57	44	41	46	52
Nb	19	19	17	18	18	19	15
Nd	36	34	38	38	37	36	31
Ni	3	3	3	3	4	3	3
Pb	22	23	25	19	19	19	25
Rb	110	111	130	96	91	96	110
Sc	6	6	3	9	10	8	4
Sr	305	296	97	488	528	479	198
Th	11	12	14	11	9	9	11
U	3	3	5	6	2	3	3
V	9	7	2	36	50	29	3
Y	25	26	22	26	25	27	19
Zn	68	69	56	79	82	78	59
Zr	392	413	311	309	287	313	350

Table 2
(continued)

Sample	BB-2011-01	BB-2011-02	BB-2011-03	BB-2011-18	BB-2011-23	BB-2012-14	BB-2012-15
Magma group	Negit Island	Negit Island	Negit Island	Negit Island	Negit Island	Negit Island	Negit Island
UTM	11S 0321345/4211192	11S 0320829/4211181	11S 0320985/4211108	11S 0320116/4209814	11S 0314795/4205740	11S 0320302/4210218	11S 0320043/4209970
SiO_2	68.06	68.81	68.71	63.45	66.62	65.38	64.68
TiO_2	0.43	0.43	0.43	0.94	0.21	0.77	0.80
Al_2O_3	15.68	15.80	15.73	16.46	13.73	16.50	16.34
FeO_T	2.83	2.83	2.82	4.68	2.04	4.05	4.22
MnO	0.07	0.07	0.07	0.09	0.06	0.08	0.08
MgO	0.56	0.56	0.56	1.47	3.43	1.15	1.22
CaO	1.95	1.95	1.95	3.71	1.11	3.19	3.22
Na_2O	4.68	4.71	4.69	4.67	4.00	4.71	4.66
K_2O	4.35	4.39	4.38	3.34	4.31	3.56	3.63
P_2O_5	0.13	0.13	0.13	0.34	0.06	0.28	0.28
Total	98.76	99.68	99.45	99.14	95.58	99.67	99.14
Ba	1250	1218	1228	1327	898	1402	1303
Ce	81	84	83	61	86	68	70
Cr	4	3	2	2	3	1	2
Cu	1	3	3	7	14	6	8
Ga	18	19	20	20	16	21	20
La	44	46	48	34	49	34	36
Nb	14	14	14	13	14	12	13
Nd	29	31	30	29	28	26	30
Ni	3	3	3	3	4	2	2
Pb	22	23	22	17	23	18	19
Rb	100	102	101	75	98	80	81
Sc	5	5	4	8	3	8	8
Sr	306	303	302	521	142	480	459
Th	10	10	11	7	11	6	7
U	2	3	2	3	1	4	2
V	12	14	11	68	4	46	52
Y	18	19	20	20	18	19	20
Zn	61	62	62	76	51	71	71
Zr	312	312	311	261	325	263	274

Table 2
(continued)

Sample	83083-1 [1]	BB-2011-15c-1	BB-2011-15c-2	LV87-1 [1]	VGC-1 [1]	BB-2011-05b-1	BB-2011-05b-2
Magma group	Inyo enclaves	Inyo enclaves	Inyo enclaves	Inyo enclaves	Inyo enclaves	Dome 14 enclaves	Dome 14 enclaves
UTM		11S 0322210/4176138	11S 0322210/4176138			11S 0322199/4195444	11S 0322199/4195444
SiO_2	58.50	59.65	59.90	59.70	57.30	56.17	54.86
TiO_2	0.91	0.76	1.33	0.98	0.92	1.93	1.75
Al_2O_3	15.40	17.26	16.27	16.30	17.00	15.73	16.28
FeO_T	5.80	4.67	5.82	6.03	5.66	8.62	8.34
MnO	0.18	0.11	0.15	0.17	0.11	0.15	0.15
MgO	3.13	3.06	2.16	3.3.8	2.74	3.92	4.63
CaO	4.99	5.81	4.32	5.31	5.33	6.53	6.71
Na_2O	4.65	4.17	4.77	4.50	4.11	3.98	4.02
K_2O	2.46	2.54	2.93	2.61	2.90	2.24	2.10
P_2O_5	0.30	0.18	0.41	0.23	0.35	0.44	0.39
Total	96.32	98.21	98.07	95.83	96.42	99.71	99.22
Ba	464	676	650	477	937	413	378
Ce		49	84			64	61
Cr	12	15	3	49	6	37	41
Cu	15	8	16	10	9	23	30
Ga		18	20			21	20
La		23	30			32	29
Nb	27	8	19	29	26	19	19
Nd		21	41			32	26
Ni	22	25	4	31	14	28	46
Pb		15	18			10	9
Rb	77	72	75	80	89	60	52
Sc		12	12			20	20
Sr	492	583	371	483	873	446	452
Th		5	8			8	6
U		2	2			3	3
V		93	145			179	154
Y	11	16	29	14	10	31	30
Zn	110	65	102	100	83	92	96
Zr	187	150	241	182	167	217	230

Table 2
(continued)

Sample	BB-2012-02b-1	BB-2012-02b-2	M14-1B [2]	BB-2012-03b-1	BB-2012-03b-2	M12-1B [2]	M12-2B [2]
Magma group	Dome 14 enclaves	Dome 14 enclaves	Dome 14 enclaves	Dome 12 enclaves	Dome 12 enclaves	Dome 12 enclaves	Dome 12 enclaves
UTM	11S 0322262/4195540	11S 0322262/4195540		11S 0321340/4196196	11S 0321340/4196196		
SiO_2	59.68	59.29	57.85	50.06	52.68	54.59	52.60
TiO_2	1.40	1.43	1.49	2.38	2.09	0.94	2.08
Al_2O_3	15.51	15.92	15.87	17.26	17.12	17.46	17.48
FeO_T	6.99	6.96	8.02	11.02	9.59	9.23	10.15
MnO	0.13	0.13		0.19	0.16		
MgO	3.58	3.66	4.04	5.09	5.00	4.47	4.25
CaO	5.36	5.64	5.84	8.49	7.84	7.76	7.64
Na_2O	4.04	4.01	3.84	3.73	3.65	3.38	3.79
K_2O	2.66	2.62	2.55	1.25	1.48	1.66	1.58
P_2O_5	0.32	0.33	0.37	0.43	0.39	0.39	0.31
Total	99.68	100.00	99.87	99.90	100.00	99.88	99.88
Ba	283	311	303	429	383	358	444
Ce	62	62	59	52	44	45	47
Cr	32	32	39	29	25	19	10
Cu	21	21		34	31		
Ga	21	20		22	22		
La	31	29	27	24	18	20	21
Nb	19	20	22	18	18	18	19
Nd	30	28	29	30	26	22	27
Ni	35	35	35	36	34	27	21
Pb	13	13		4	9		
Rb	82	78	71	33	35	45	35
Sc	17	15	15	26	23	19	18
Sr	348	374	374	643	588	592	643
Th	9	9		3	4		
U	3	3		2	4		
V	131	127	136	249	212	197	196
Y	30	30	32	33	27	25	26
Zn	81	80		112	99		
Zr	207	209	212	188	168	159	171

Table 2 (continued)

Sample	BB-2012-05b-1	BB-2012-05b-2	BB-2012-05b-3	M18-1B [2]	BB-2012-04b
Magma group	Dome 18 enclaves	Dome 18 enclaves	Dome 18 enclaves	Dome 18 enclaves	N. Deadman enclaves
UTM					11S 0321865/4176572
SiO_2	55.01	56.46	60.44	61.73	61.63
TiO_2	1.81	1.64	1.32	1.20	1.03
Al_2O_3	16.57	16.18	15.38	15.31	16.31
FeO_T	8.60	8.02	6.49	6.63	5.51
MnO	0.15	0.14	0.12		0.10
MgO	4.73	4.48	3.53	3.01	2.11
CaO	6.96	6.58	5.28	4.82	4.15
Na_2O	4.04	3.96	3.90	3.99	4.38
K_2O	2.04	2.22	2.81	2.96	3.38
P_2O_5	0.42	0.47	0.29	0.27	0.24
Total	100.34	100.15	99.57	99.92	98.83
Ba	379	315	255	298	961
Ce	70	62	61	62	63
Cr	39	52	40	26	5
Cu	23	20	18		9
Ga	21	20	20		21
La	31	28	28	31	33
Nb	19	20	19	21	14
Nd	31	31	27	29	27
Ni	43	43	34	30	6
Pb	9	10	15		16
Rb	52	59	85	87	81
Sc	21	18	16	12	11
Sr	465	419	331	308	405
Th	6	7	10		9
U	4	4	3		2
V	168	153	123	111	103
Y	31	31	30	30	22
Zn	92	89	134		73
Zr	231	211	195	198	290

[1] Data from Varga et al. (1990).
[2] Data from Kelleher and Cameron (1990).

Table 3

Table 3: Isotopic compositions of the Mono Basin lavas.

Sample	Magma group	$^{87}Sr/^{86}Sr_i$	$^{143}Nd/^{144}Nd$	ε_{Nd}	$^{206}Pb/^{204}Pb$	$^{207}Pb/^{204}Pb$	$^{208}Pb/^{204}Pb$	$\delta^{18}O$
BB-2011-22	Basalt	0.706160 [1]	0.512580 [1]		19.250 [1]	15.670 [1]	38.890 [1]	7.42
BB-2011-24	Basalt	0.705380 [1]	0.512670 [1]		19.220 [1]	15.660 [1]	38.830 [1]	7.95
BB-2012-03b-1	Dome 12 enclaves	0.704869	0.512758	2.34	19.137	15.672	38.869	7.79
BB-2011-05b-2	Dome 14 enclaves	0.704535	0.512785	2.87	19.094	15.665	38.864	6.82
BB-2012-02b-2	Dome 14 enclaves	0.704520	0.512749	2.17	19.122	15.668	38.886	6.89
BB-2012-05b-1	Dome 18 enclaves	0.704421	0.512779	2.75	19.105	15.674	38.895	12.68
BB-2012-05b-3	Dome 18 enclaves	0.704516	0.512754	2.26	19.114	15.661	38.865	7.15
BB-2011-14	Mono domes	0.706024	0.512602	-0.70	19.127	15.666	38.902	9.02
BB-2011-20	Mono domes	0.705960	0.512614	-0.47	19.138	15.677	38.939	6.91
BB-2012-05	Mono domes	0.706905	0.512618	-0.39	19.173	15.697	39.008	7.73
BB-2012-04b	N. Deadman enclaves	0.705640	0.512646	0.16	19.174	15.673	38.920	7.97
BB-2011-01	Negit Island	0.706239	0.512537	-1.97	19.209	15.696	38.992	7.73
BB-2011-23	Negit Island	0.706209	0.512581	-1.11	19.186	15.690	38.978	8.82
BB-2012-14	Negit Island	0.706429	0.512527	-2.16	19.240	15.709	39.036	8.11
BB-2011-10	Paoha Island	0.705998	0.512571	-1.31	19.176	15.707	39.033	9.44
BB-2011-11	Paoha Island	0.706094	0.512594	-0.86	19.172	15.686	38.968	11.55
BB-2011-16	Paoha Island	0.705873	0.512563	-1.46	19.153	15.689	38.970	7.58
BB-2011-15c-2	Inyo enclaves	0.706225	0.512520	-2.30	19.202	15.694	38.977	6.89

[1] Sr, Nd, and Pb data for the Black Point and June Lake basalts from Cousens (1996)

Table 4a: Electron microprobe analyses of Mono Basin glasses. Major elements reported in wt.%.

Sample	09112013_BB-2012-17_Glass_1	09112013_BB-2012-17_Glass_3	09112013_BB-2012-17_Glass_4	09112013_BB-2012-17_Glass_5	BB-2011-05_Glass_2	BB-2011-05_Glass_3	BB-2011-05_Glass_4
Magma group	Mono domes	Mono domes	Mono domes	Mono domes	Mono domes	Mono domes	Mono domes
SiO_2	74.41	75.87	76.52	76.10	54.94	48.49	50.92
TiO_2	0.07	0.00	0.06	0.06	1.80	3.13	3.47
Al_2O_3	11.97	12.42	12.49	13.56	15.03	16.31	16.73
FeO_T	0.67	0.82	0.79	0.74	8.61	11.07	8.62
MnO	0.03	0.00	0.05	0.01	0.22	0.18	0.18
MgO	0.00	0.00	0.01	0.00	3.40	4.20	4.00
CaO	0.45	0.45	0.46	0.61	8.89	8.74	9.21
Na_2O	3.89	3.89	3.90	4.53	4.52	4.12	4.18
K_2O	4.64	4.58	4.68	4.43	1.72	1.52	1.34
P_2O_5	0.00	0.00	0.04	0.01	0.57	0.65	0.63
Total	96.13	98.03	99.00	100.05	99.70	98.40	99.27

Table 4a (continued)

Sample	BB-2011-05_Glass_5	BB-2011-05_Glass_6	BB-2012-11b_Glass_1	BB-2012-11b_Glass_2	BB-2012-11b_Glass_3	BB-2012-11b_Glass_4	BB-2012-11b_Glass_5
Magma group	Mono domes	Mono domes	Mono domes	Mono domes	Mono domes	Mono domes	Mono domes
SiO_2	52.17	76.20	75.05	76.23	76.42	75.89	75.73
TiO_2	2.49	0.10	0.06	0.05	0.12	0.03	0.00
Al_2O_3	15.73	12.45	11.85	12.46	12.48	12.43	12.52
FeO_T	9.73	0.87	0.74	0.85	0.93	0.94	0.82
MnO	0.34	0.06	0.06	0.05	0.02	0.04	0.06
MgO	3.85	0.02	0.01	0.02	0.01	0.03	0.00
CaO	9.58	0.46	0.51	0.55	0.52	0.53	0.46
Na_2O	4.10	4.02	3.78	4.08	4.00	4.03	4.08
K_2O	1.32	4.91	4.62	4.58	4.84	4.67	4.66
P_2O_5	0.50	0.00	0.00	0.02	0.01	0.00	0.00
Total	99.79	99.08	96.68	98.87	99.34	98.57	98.32

Table 4a (continued)

Sample	BB-2012-11b_Glass_6	BB-2012-16_Glass_1	BB-2012-16_Glass_2	BB-2012-16_Glass_3	BB-2012-16_Glass_6	09112013_BB-2011-10_Glass_1	09112013_BB-2011-10_Glass_10
Magma group	Mono domes	Mono domes	Mono domes	Mono domes	Mono domes	Paoha Island	Paoha Island
SiO_2	76.43	75.79	75.51	74.78	74.19	67.23	70.20
TiO_2	0.09	0.02	0.00	0.02	0.05	0.42	0.44
Al_2O_3	12.55	12.46	12.44	12.13	11.99	18.07	15.92
FeO_T	0.86	0.70	0.84	0.69	0.82	1.19	1.65
MnO	0.04	0.07	0.03	0.05	0.04	0.06	0.06
MgO	0.01	0.01	0.01	0.00	0.00	0.09	0.15
CaO	0.55	0.52	0.54	0.46	0.53	2.25	1.12
Na_2O	4.20	4.12	4.06	3.96	3.93	6.24	5.30
K_2O	4.72	4.63	4.45	4.58	4.45	3.83	5.14
P_2O_5	0.05	0.00	0.00	0.00	0.00	0.13	0.12
Total	99.48	98.31	97.88	96.66	96.03	99.50	100.09

Table 4a (continued)

Sample	09112013_BB-2011-10_Glass_11	09112013_BB-2011-10_Glass_2	09112013_BB-2011-10_Glass_3	09112013_BB-2011-10_Glass_4	09112013_BB-2011-10_Glass_5	09112013_BB-2011-10_Glass_6	09112013_BB-2011-10_Glass_7
Magma group	Paoha Island	Paoha Island	Paoha Island	Paoha Island	Paoha Island	Paoha Island	Paoha Island
SiO_2	69.29	68.38	66.51	69.15	69.52	69.04	64.06
TiO_2	0.32	0.53	0.52	0.55	0.66	0.47	0.70
Al_2O_3	17.15	16.58	17.77	16.64	14.57	14.55	16.54
FeO_T	1.20	1.50	2.10	1.32	2.83	3.00	4.40
MnO	0.04	0.02	0.02	0.00	0.08	0.17	0.13
MgO	0.07	0.25	0.30	0.13	0.61	1.01	1.27
CaO	1.88	1.76	2.56	1.60	0.86	1.11	3.32
Na_2O	5.80	5.74	6.44	5.70	4.49	4.54	5.41
K_2O	4.36	4.46	3.46	4.78	5.86	5.26	3.70
P_2O_5	0.13	0.16	0.13	0.18	0.17	0.16	0.89
Total	100.23	99.38	99.81	100.05	99.65	99.31	100.41

Table 4a (continued)

Sample	09112013_BB-2011-10_Glass_8	09112013_BB-2011-10_Glass_9	BB-2011-10_Glass_3	BB-2011-10_Glass_4	BB-2011-10_Glass_5	BB-2011-10_Glass_7	BB-2011-10_Glass_8
Magma group	Paoha Island	Paoha Island	Paoha Island	Paoha Island	Paoha Island	Paoha Island	Paoha Island
SiO_2	69.81	68.87	67.25	69.23	70.71	68.77	71.06
TiO_2	0.44	0.77	0.33	0.73	0.40	0.37	0.40
Al_2O_3	15.34	13.95	16.34	14.35	14.23	15.44	15.06
FeO_T	1.67	5.53	2.03	2.08	1.89	2.57	1.48
MnO	0.05	0.09	0.05	0.05	0.07	0.10	0.04
MgO	0.23	0.15	0.54	0.12	0.28	0.68	0.13
CaO	1.21	0.56	2.12	1.06	0.75	1.64	1.10
Na_2O	5.03	4.37	5.62	4.50	4.63	5.11	4.86
K_2O	5.27	5.72	4.11	5.46	5.49	4.70	5.17
P_2O_5	0.04	0.09	0.23	0.26	0.10	0.08	0.06
Total	99.10	100.10	98.63	97.83	98.54	99.47	99.37

Table 4a (continued)

Sample	BB-2011-17_Glass_2	BB-2011-17_Glass_3	BB-2011-17_Glass_5	BB-2011-18_Glass_2	BB-2011-18_Glass_3	BB-2011-18_Glass_4	BB-2011-18_Glass_5
Magma group	Paoha Island	Paoha Island	Paoha Island	Negit Island	Negit Island	Negit Island	Negit Island
SiO_2	70.94	71.26	70.81	65.84	66.18	69.82	64.85
TiO_2	0.16	0.19	0.14	0.71	0.68	0.81	0.90
Al_2O_3	14.57	14.84	14.69	16.80	17.07	14.99	15.99
FeO_T	1.75	2.03	1.95	2.78	2.45	2.03	4.05
MnO	0.06	0.05	0.08	0.05	0.07	0.04	0.07
MgO	0.16	0.13	0.15	0.50	0.58	0.17	1.48
CaO	1.04	1.08	1.05	3.05	3.28	1.66	3.28
Na_2O	4.48	4.61	4.53	5.04	5.24	4.62	4.66
K_2O	5.19	5.11	5.14	3.56	3.72	4.86	3.61
P_2O_5	0.07	0.00	0.06	0.22	0.31	0.21	0.37
Total	98.43	99.29	98.59	98.55	99.58	99.20	99.24

Table 4a (continued)

Sample	BB-2011-05b-2_Glass_3	BB-2011-05b-2_Glass_6	BB-2011-05b-2_Glass_8
Magma group	Dome 14 enclaves	Dome 14 enclaves	Dome 14 enclaves
SiO_2	76.44	64.73	59.90
TiO_2	0.03	0.84	0.56
Al_2O_3	12.95	16.11	15.13
FeO_T	0.72	3.58	5.69
MnO	0.04	0.04	0.13
MgO	0.04	0.90	3.73
CaO	0.31	1.35	6.15
Na_2O	3.11	4.62	5.81
K_2O	5.92	5.78	1.59
P_2O_5	0.00	0.15	0.76
Total	99.56	98.11	99.44

Table 4b: Electron microprobe analyses of Mono Basin amphiboles. Major elements reported in wt.%.

Sample	BB201110-C1-1	BB201110-C1-2	BB201110-C5-1	BB201110-C6-1	BB201110-C7-1	BB-2011-12_amph_1	BB-2011-12_amph_2
Magma group	Paoha Island	Paoha Island	Paoha Island	Paoha Island	Paoha Island	Paoha Island	Paoha Island
SiO_2	42.14	42.83	42.87	41.69	42.36	42.19	42.14
TiO_2	3.869	3.422	3.428	3.769	3.750	3.832	3.955
Al_2O_3	10.61	10.37	10.32	10.47	10.70	10.88	11.14
FeO_T	12.65	12.78	13.60	12.82	12.96	13.06	13.48
MnO	0.259	0.247	0.281	0.246	0.225	0.226	0.237
MgO	13.42	13.67	13.39	13.27	13.13	13.68	13.25
CaO	10.88	10.89	10.47	11.17	10.84	10.93	10.91
Na_2O	2.475	2.495	2.423	2.519	2.568	2.562	2.509
K_2O	0.913	0.960	0.921	0.869	0.943	0.977	0.957
Cr_2O_3	0.000	0.000	0.007	0.000	0.000	0.000	0.000
Cl	0.016	0.004	0.019	0.000	0.004	0.007	0.002
F	0.252	0.319	0.306	0.307	0.294	0.173	0.390
Total	97.37	97.85	97.90	96.99	97.64	98.45	98.81

Table 4b (continued)

Sample	BB-2011-12_amph_3	BB-2011-12_amph_4	BB-2011-12_amph_5	BB-2011-17_amph_1	BB-2011-17_amph_3	BB-2011-17_amph_4	BB-2011-17_amph_5
Magma group	Paoha Island	Paoha Island	Paoha Island	Paoha Island	Paoha Island	Paoha Island	Paoha Island
SiO_2	41.67	41.92	42.32	42.40	42.61	42.44	42.44
TiO_2	3.992	4.031	3.795	3.359	3.249	2.961	3.197
Al_2O_3	10.98	10.93	10.90	10.82	10.90	10.66	10.89
FeO_T	13.04	13.08	13.18	14.36	14.46	15.66	15.64
MnO	0.225	0.215	0.246	0.222	0.274	0.260	0.259
MgO	12.78	13.34	13.48	12.43	11.64	12.09	11.91
CaO	10.96	11.04	10.95	10.79	10.77	10.61	10.56
Na_2O	2.509	2.548	2.545	2.363	2.443	2.356	2.351
K_2O	1.012	0.989	0.953	0.851	0.906	0.920	0.912
Cr_2O_3	0.000	0.016	0.000	0.000	0.000	0.000	0.010
Cl	0.013	0.004	0.029	0.019	0.025	0.012	0.033
F	0.405	0.585	0.280	0.229	0.004	0.220	0.224
Total	97.41	98.46	98.56	97.75	97.26	98.10	98.31

Table 4b (continued)

Sample	BB-2011-17_amph_6	BB-2011-15_amph_1	BB-2011-15_amph_2	BB-2011-15_amph_3	BB-2011-15_amph_4	BB-2011-15_amph_5	BB-2011-15_amph_6
Magma group	Paoha Island	Inyo domes	Inyo domes	Inyo domes	Inyo domes	Inyo domes	Inyo domes
SiO_2	42.56	47.20	44.00	42.95	47.98	46.82	45.65
TiO_2	3.324	1.202	2.468	2.869	1.163	1.276	1.670
Al_2O_3	10.91	6.267	8.786	9.429	5.654	6.709	7.313
FeO_T	13.69	16.52	17.45	17.18	15.72	16.24	17.19
MnO	0.218	0.657	0.609	0.639	0.634	0.651	0.664
MgO	11.99	12.44	10.97	10.85	13.59	12.93	11.85
CaO	11.15	11.45	11.22	11.17	11.33	11.50	11.22
Na_2O	2.379	1.444	1.973	2.091	1.315	1.553	1.682
K_2O	0.896	0.685	0.853	0.794	0.565	0.782	0.835
Cr_2O_3	0.006	0.000	0.000	0.027	0.000	0.000	0.000
Cl	0.017	0.043	0.046	0.037	0.042	0.061	0.068
F	0.285	0.077	0.128	0.167	0.233	0.193	0.187
Total	97.30	97.94	98.44	98.13	98.11	98.63	98.24

Table 4b (continued)

Sample	BB-2011-15_amph_7	BB-2011-15_amph_8	BB-2011-15_amph_9	BB-2011-15_amph_10	BB-2011-15_amph_11	BB-2011-15_amph_12	BB-2011-15_amph_13
Magma group	Inyo domes	Inyo domes	Inyo domes	Inyo domes	Inyo domes	Inyo domes	Inyo domes
SiO_2	46.56	46.45	46.27	45.72	45.55	45.58	45.54
TiO_2	1.366	1.394	1.483	1.462	1.519	1.652	1.650
Al_2O_3	6.985	6.854	7.347	7.439	7.405	7.500	7.370
FeO_T	17.00	16.60	16.59	17.31	17.28	16.44	16.41
MnO	0.674	0.672	0.599	0.643	0.592	0.605	0.579
MgO	12.31	12.24	12.54	11.95	11.53	12.66	12.57
CaO	11.31	11.25	11.35	11.32	11.22	11.25	11.15
Na_2O	1.668	1.574	1.682	1.702	1.643	1.683	1.686
K_2O	0.792	0.736	0.838	0.899	0.880	0.903	0.852
Cr_2O_3	0.019	0.000	0.000	0.000	0.000	0.000	0.000
Cl	0.042	0.053	0.040	0.048	0.062	0.068	0.067
F	0.197	0.274	0.055	0.249	0.320	0.400	0.254
Total	98.82	97.97	98.76	98.62	97.84	98.56	97.99

Table 4b (continued)

Sample	BB-2011-15_amph_14	BB-2011-15_amph_15	BB-2011-15_amph_16	BB-2011-15c-1_amph_1	BB-2011-15c-1_amph_2	BB-2011-15c-1_amph_3	BB-2011-15c-1_amph_4
Magma group	Inyo domes	Inyo domes	Inyo domes	Inyo enclaves	Inyo enclaves	Inyo enclaves	Inyo enclaves
SiO_2	46.58	45.03	45.60	47.44	45.29	45.39	45.74
TiO_2	1.512	1.639	1.646	1.278	1.575	1.599	1.405
Al_2O_3	7.436	7.720	7.430	5.742	6.898	7.201	6.850
FeO_T	15.98	16.58	16.43	15.21	16.98	16.81	16.58
MnO	0.577	0.563	0.561	0.435	0.693	0.630	0.652
MgO	12.19	12.64	12.87	13.93	12.61	12.25	12.32
CaO	11.03	11.17	11.19	11.20	10.86	11.01	11.26
Na_2O	1.747	1.768	1.715	1.425	1.558	1.693	1.550
K_2O	1.063	0.925	0.840	0.648	0.757	0.805	0.766
Cr_2O_3	0.000	0.000	0.000	0.000	0.005	0.000	0.021
Cl	0.059	0.037	0.046	0.028	0.057	0.064	0.071
F	0.236	0.395	0.153	0.092	0.239	0.282	0.249
Total	98.28	98.29	98.41	97.38	97.41	97.60	97.33

Table 4b (continued)

Sample	BB-2011-15c-1_amph_5	BB-2011-15c-1_amph_6	BB-2011-15c-1_amph_7	BB-2011-15c-1_amph_8	BB-2011-15c-1_amph_9	BB-2011-15c-1_amph_10	BB-2011-18_amph_1
Magma group	Inyo enclaves	Inyo enclaves	Inyo enclaves	Inyo enclaves	Inyo enclaves	Inyo enclaves	Negit Island
SiO_2	46.78	43.17	43.96	46.30	43.86	43.62	41.21
TiO_2	1.283	2.503	1.771	1.272	1.866	2.197	4.073
Al_2O_3	6.451	10.42	9.222	5.512	9.273	9.822	11.35
FeO_T	16.00	13.99	14.59	17.23	15.48	15.35	12.84
MnO	0.606	0.290	0.367	0.660	0.460	0.464	0.159
MgO	12.74	12.38	13.11	13.24	12.65	11.75	13.23
CaO	11.24	11.42	11.35	10.69	11.17	11.17	11.08
Na_2O	1.526	2.263	2.013	1.425	2.030	2.182	2.346
K_2O	0.701	0.846	0.798	0.605	0.809	0.782	0.790
Cr_2O_3	0.019	0.000	0.000	0.029	0.000	0.000	0.000
Cl	0.049	0.033	0.028	0.063	0.035	0.048	0.008
F	0.175	0.244	0.227	0.344	0.206	0.111	0.025
Total	97.49	97.45	97.33	97.21	97.74	97.44	97.10

Table 4b (continued)

Sample	BB-2012-15_amph_1	BB-2012-15_amph_2
Magma group	Negit Island	Negit Island
SiO_2	41.99	42.00
TiO_2	3.681	3.578
Al_2O_3	10.98	10.67
FeO_T	12.89	13.19
MnO	0.213	0.214
MgO	13.90	13.86
CaO	11.17	11.02
Na_2O	2.443	2.450
K_2O	0.761	0.764
Cr_2O_3	0.000	0.020
Cl	0.016	0.013
F	0.000	0.212
Total	98.04	97.90

ESM Table 1b

ESM Table 1c

Click here to access/download
Supplementary Material
ESM Table 1c.docx

ESM Table 2

Click here to access/download
Supplementary Material
ESM Table 2.docx

ESM Table 3

ESM Figure 1